



The origin of continental carbonates in Andean salars: a multi-tracer geochemical approach in Laguna Pastos Grandes (Bolivia).

E. Muller, E.C. Gaucher, Christophe Durlet, J.S. Moquet, M. Moreira, V. Rouchon, P. Louvat, Gérard Bardoux, S. Noirez, Cédric Bougeault, et al.

► To cite this version:

E. Muller, E.C. Gaucher, Christophe Durlet, J.S. Moquet, M. Moreira, et al.. The origin of continental carbonates in Andean salars: a multi-tracer geochemical approach in Laguna Pastos Grandes (Bolivia).. *Geochimica et Cosmochimica Acta*, 2020, 279, pp.220-237. 10.1016/j.gca.2020.03.020 . hal-02860683

HAL Id: hal-02860683

<https://hal.science/hal-02860683>

Submitted on 9 Jun 2020

HAL is a multi-disciplinary open access archive for the deposit and dissemination of scientific research documents, whether they are published or not. The documents may come from teaching and research institutions in France or abroad, or from public or private research centers.

L'archive ouverte pluridisciplinaire **HAL**, est destinée au dépôt et à la diffusion de documents scientifiques de niveau recherche, publiés ou non, émanant des établissements d'enseignement et de recherche français ou étrangers, des laboratoires publics ou privés.

**The Origin of Continental Carbonates in Andean Salars:
A Multi-Tracer Geochemical Approach in Laguna Pastos Grandes (Bolivia)**

E. Muller¹, E. C. Gaucher², C. Durllet³, J.S. Moquet¹, M. Moreira¹, V. Rouchon⁴, P. Louvat¹, G. Bardoux¹, S. Noirez⁴, C. Bougeault³, E. Vennin³, E. Gérard¹, M. Chavez⁵, A. Virgone², M. Ader¹

¹Université de Paris, Institut de physique du globe de Paris, CNRS, F-75005 Paris, France

²Total CSTJF, Avenue Larribau, 64018 Pau Cedex, France

³Biogéosciences, UMR 6282 CNRS, 6 boulevard Gabriel, Université Bourgogne Franche-Comté, 21000 Dijon, France

⁴IFP Energies Nouvelles, 1-4 Avenue de Bois Préau, 92852, Rueil-Malmaison Cedex, France

⁵Total E&P, 40 Calle Las Violetas, Edificio Arcus, Santa Cruz de la Sierra, Bolivia

Corresponding author: Elodie Muller (emuller@ipgp.fr)

This article has been accepted in *Geochimica et Cosmochimica Acta*.

Abstract

In continental volcanic settings, abundant carbonate precipitation can occur with atypical facies compared to marine settings. The (bio-)chemical processes responsible for their development and early diagenesis are typically complex and not fully understood. In the Bolivian Altiplano, Laguna Pastos Grandes hosts a 40-km² carbonate platform with a great diversity of facies and provides an ideal natural laboratory to understand the processes responsible for the precipitation of carbonates in a continental province dominated by volcanism. In order to trace the origin of both water and solutes in the lagoon, the major element and stable isotope compositions ($\delta^2\text{H}$ - $\delta^{18}\text{O}$, $\delta^{37}\text{Cl}$, $\delta^7\text{Li}$, $\delta^{11}\text{B}$ and $^{87}\text{Sr}/^{86}\text{Sr}$) of the spring and stream waters were characterized, as well as the stable isotope compositions ($\delta^{13}\text{C}$, $\delta^{15}\text{N}$) and noble gas isotope ratios of hydrothermal gases associated with spring waters. The results show that thermal springs discharging on the carbonate platform are close to saturation with calcite. PHREEQC modeling, together with fluid geochemistry and temperature estimated from a combination of geothermometers, indicate that Ca in these springs is inherited from the alteration of the volcanic bedrock by aqueous fluids heated at ~225 °C and enriched in magmatic mantle-derived CO₂. Our results clearly show that the main driver for the precipitation of modern carbonates in Laguna Pastos Grandes is the deeply sourced CO₂, which boosts the alteration of volcanic rocks at depth.

1. Introduction

It has long been documented that continental carbonates can form, in varying abundances, both in pedogenetic profiles (see synthesis in Zamanian et al., 2016; Durand et al., 2018) and in palustrine-lacustrine environments (see synthesis in Alonso-Zarza and Tanner, 2010; Verrecchia, 2007). Yet, their occurrences in continental volcanic provinces, typically

dominated by volcanoclastic, bio-silica, clay or evaporitic sediments, have not been investigated as much as their marine equivalents, generally considered as common hydrocarbon reservoirs and traditional archives of past oceans since the Archean. The recent discovery of hydrocarbon plays in Lower Cretaceous continental carbonates off the Brazilian coast changed this paradigm (Terra et al., 2010; Tosca and Wright, 2015) and promoted several studies focused on the origin and occurrence of carbonates in continental settings where the catchment and underlying rocks are mainly volcanic (e.g., Teboul et al., 2016; 2017).

Laguna Pastos Grandes in southern Bolivia includes a ~40 km² carbonate platform making it unique among the more than 200 salars scattered across the volcanic Central Andes region (Fig. 1a, b). Laguna Negra in Argentina is the only other Andean salar recently described with a significant, but much smaller (6.5 km²; Gomez et al., 2014), carbonate platform. Laguna Pastos Grandes exhibits a great diversity of calcitic, siliceous and evaporitic fabrics deposited in palustrine to shallow lacustrine environments, including some of the largest modern pisoliths discovered to date (Fig. 1c; Risacher and Eugster, 1979; Jones and Renaut, 1994; Bougeault et al., 2019). In some ways, it may be considered as a modern equivalent of carbonate facies and processes that occurred during sedimentation of the Presalt facies in the volcanic-rich South Atlantic realm during the Early Cretaceous.

Although several studies were conducted on the hydrology and origin of chemical sediments in Bolivian and Chilean salars, a clear explanation for the abundance of modern carbonates in Laguna Pastos Grandes is still lacking. From structural, climatic and lithological points of view, Laguna Pastos Grandes seems to be similar to salars where carbonate precipitation is insignificant (Risacher et al., 2003; Risacher and Fritz, 2009; see geological setting). Indeed, while climatic parameters fundamentally control the existence and morphology of salars (Risacher and Fritz, 2009), the chemical composition of the brines and the nature of the precipitates in these lakes mainly depend on the initial composition of the inflow waters. In the present study, we thus performed a comprehensive geochemical study of gases and waters discharging on the carbonate platform of Laguna Pastos Grandes and of the brine filling the main basin.

The overarching goal of our research is to better understand the ongoing processes that allow for the rapid growth of these continental carbonates in a volcanic area under structural extension and fed by hydrothermal fluids. As a first step, this study focuses on the origin of the fluids and solutes from which carbonates have formed in the laguna based on the study of: (i) the chemical compositions of water samples from streams of the drainage area and hydrothermal springs upwelling through or near the carbonate platform and gas associated with the hydrothermal springs; (ii) the isotopic compositions of gas components ($\delta^{13}\text{C}$, $\delta^{15}\text{N}$ and noble gases), water samples ($\delta^2\text{H}$ and $\delta^{18}\text{O}$) and some of their solutes ($\delta^{37}\text{Cl}$, $\delta^7\text{Li}$, $\delta^{11}\text{B}$ and $^{87}\text{Sr}/^{86}\text{Sr}$); and (iii) Li, B and Sr isotopic compositions of volcanic rock samples surrounding the salar. These results, together with the temperature of the underlying geothermal reservoir estimated from a combination of geothermometers and with PHREEQC modeling of the hydrological system allowed us to identify the main

factor responsible for the abundant precipitation of modern carbonates in Laguna Pastos Grandes.

2. Geological Setting

Laguna Pastos Grandes is located in the southern part of the Bolivian Altiplano, in the South Lipez region. The Altiplano (3700 – 4500 m) is a major Plio-Pleistocene continental plateau bounded by the Eastern and Western Cordilleras and dominated by Cenozoic stratovolcanoes and their products (Fig. 1). To the south, rhyolitic ignimbrites and dacites to rhyodacites of the Altiplano-Puna Volcanic Complex (APVC) dominate the South Lipez region, whereas andesites to dacites predominate on the Chilean side (Thorpe et al., 1976). Native sulfur deposits occur on many volcanoes in Chile, and thermal springs are abundant. A thick succession of Cretaceous and Tertiary continental sediments, including evaporite deposits, outcrops in the Bolivian Eastern Cordillera and could be covered by volcanic rocks towards the west in the studied area (Deconinck et al., 2000).

There are more than 200 closed basin lakes in the Bolivian Altiplano and Chilean Western Cordillera (Luddington et al., 1992). Most are saline and encompass a wide range of perennial or ephemeral lakes, locally termed “salars”. The two largest salars, Uyuni and Coipasa, are remnants of larger Pleistocene lakes and occupy the lower part of the Altiplano (3650 m altitude), whereas an abundance of smaller evaporitic basins (<400 km²) occur at higher altitudes (4000–4500 m) of the southern Altiplano (Fig. 1). The presence of these southern basins and their morphology primarily result from the cold and dry climate of this region, characterized by mean annual precipitations between 100 and 200 mm, air temperatures varying from -30 °C in winter to 25 °C in summer with daytime fluctuations of up to 40 °C, and annual evaporation of about 1400 mm (Risacher and Fritz, 1991). Although they belong to relatively similar environments in terms of geology and climate, Andean salars show a wide variety of brine compositions, which can be organized into three major groups: alkaline, sulfate-rich, and calcium-rich brines (Risacher and Fritz, 2009). Different precipitates can be found in association with these brines, the most common being sodium chloride, sodium sulfates to borates, sodium carbonates and calcium sulfates (Risacher and Fritz, 2009). Their formation and evolution are thought to result from the combination of two fundamental factors: the presence of interior drainage basins as a source of solutes and high evaporation rates allowing salt precipitation (Risacher et al., 2003). Inflows to the Andean salars stem from various sources such as permanent and ephemeral streams, shoreline springs, groundwater discharge, and thermal springs. Most of the rainwater falling on the drainage area infiltrates and recharges underlying aquifers. Shoreline spring and hot-spring waters are typically enriched in solutes compared with streams due to the dissolution of ancient and/or present-day evaporitic sediments or through the infiltration and recycling of lake brines. Therefore, the composition of inflow waters feeding Andean salars reflects a mixture from two main sources: (1) dilute waters produced by the alteration of volcanic rocks by meteoric waters and (2) highly concentrated brackish waters derived from brine/salt recycling (Risacher et al., 2003 and references therein). The high rate of evaporation of these inflow waters in ponds and lakes increases the concentration of solutes and leads to the precipitation of a sequence of minerals in the order of their increasing solubility, following diverse evaporative pathways depending on the initial chemistry of inflow waters (Risacher and Fritz, 2009).

With an area of $\sim 120 \text{ km}^2$, Laguna Pastos Grandes is one of the largest salars of the southern Altiplano (Risacher and Eugster, 1979). This salar lies at an altitude of 4450 m in a 50-km-long caldera dated at $2.89 \pm 0.01 \text{ Ma}$ by $^{40}\text{Ar}/^{39}\text{Ar}$ of sanidine (Salisbury et al., 2011) and is probably the remnant of a larger lake that once occupied the caldera moat (de Silva and Francis, 1991). The drainage basin (660 km^2) is limited to the west by rhyolitic lava ridges up to an elevation of 5800 m, and to the east by rhyolitic ignimbrite ridges up to an elevation of 5000 m (Fig. 1b). Coalescent alluvial fans with thin pebbly soils and xerophytic vegetation surround the laguna. Laguna Pastos Grandes can be divided into two main domains previously identified by Ballivian and Risacher (1981) and Jones and Renaut (1994): the eastern domain corresponds to a playa environment characterized by gypsum and carbonate muds associated with ulexite ($\text{NaCaB}_5\text{O}_6(\text{OH})_6$), and the western domain corresponds to a vast 40-km^2 palustrine carbonate platform, highly fragmented through cryoturbation exposing underlying recent carbonates (muds to calcarenites). Over these recent carbonate deposits, a few ponds no more than one decimeter deep host pisoliths and carbonate concretions up to 20 cm thick (Fig. 1c). Hydrothermal spring discharge over this platform produces important modern carbonate deposits (Bougeault et al., 2019).

3. Materials and Methods

3.1 Water, gas and rock sampling

Nine water samples were collected during two sampling trips in January 2016 and March 2017, dry and wet seasons respectively (Tables 1, 2). We thus consider our samples as representative of the two main climatic seasons in terms of rainfall. Seven samples of water were selected from five thermal springs including one on the border of the laguna, two samples from cold streams, and one sample of brine from the southwestern part of the laguna (Fig. 2, Tables 1, 2). Two samples of fresh snow and one sample of rainfall were also collected respectively in January 2016 and March 2017 in order to constrain the meteoric sources of water in the area (Table A2).

Water samples were filtered using a $0.1 \mu\text{m}$ sterile acrylic filter (Sartorius Minisart[®]) fixed at the end of a 50 mL syringe. For cation analyses, $\sim 20 \text{ ml}$ samples were acidified with 3 drops of HNO_3 (16N) in the field. The temperature and pH were measured on site at each collection point. In 2016, in the field, the total alkalinity was determined by H_2SO_4 (1.6 N) titration using a manual titrator and adapted cartridge (Hach[®]; error below 1%, Table 2; Gran, 1952). Samples of 25 ml were titrated and 25 titrations (pH and volume of added titrated acid) were numerically processed using the Gran function (Gran, 1952). The correlation factors obtained by regression on the derivate of the titration curve are better than 0.998. In 2017, the total alkalinity was determined by end-point titration with HCl (1N or 0.1N) with an automatic titrimeter (Metrohm) at the Total laboratory (France, error below 1%; Rounds and Wilde, 2012). The bicarbonates alkalinity was calculated from the total alkalinity corrected from the contribution of weak acid and $\text{B}(\text{OH})_4^-$ concentration. The $\text{B}(\text{OH})_4^-$ concentration was calculated from the B concentration (obtained with ICP-AES) and the pH of the sampled solution. The weak acid (HCOO^- ; CH_3COO^- ; $\text{C}_2\text{H}_5\text{COO}^-$; $i\text{-C}_3\text{H}_7\text{COO}^-$; $n\text{-C}_3\text{H}_7\text{COO}^-$) were measured by ionic chromatography (930 Compact IC Flex, Metrohm). Considering the high alkalinities of the samples, the contribution of OH^- remains negligible. In this article, the alkalinity refers to the $\text{HCO}_3^-/\text{CO}_3^{2-}$ alkalinity.

Four thermal springs named *La Salsa*, *La Rumba*, *El Ojo Verde* and *El Gigante* (Fig. 2) were selected for both water and gas sampling on the carbonate platform based on

accessibility and high water-gas flux. *La Salsa*, *La Rumba* and *El Ojo Verde* springs contain bubbling sources of gas in water ponds whereas *El Gigante* is a dry source of gas (a mofet) away from the main water source. Gases were collected in March 2017 in 100- and 250-mL stainless-steel reservoirs and in four 12 mL Exetainer® vials, all previously evacuated to primary vacuum. To capture bubbling thermal spring gases, an inverted funnel connected to a rubber pipe was submerged in spring water and placed on top of the rising bubbles (Fig. A1). The other end of the pipe was connected through a T-junction to a stainless-steel fitting ending in a septum (for sampling in an Exetainer®) and a stainless-steel reservoir (for direct sampling) connected to a GA5000 gas detector (Scientific Instruments). Before collecting the gases accumulated in the funnel, the sampling system was completely flushed by the continuously outgassing bubbles to avoid air contamination (O₂ level typically below 2.0%).

Five rock samples of volcanic bedrock (2 andesites, 2 dacites and 1 ignimbrite of rhyolitic composition) were also collected on the border of the laguna (see location in Fig. 2).

3.2 Analytical methods – Chemical compositions

Gas composition

The gas composition was determined on the four samples collected in Exetainer® vials with a Varian 3800 high-resolution gas chromatograph (GC) equipped with Molsieve and Haesep type chromatographic columns at the IFPEN laboratory (Rueil-Malmaison, France). H₂ and He quantification was performed using a thermal conductivity detector (TCD) with N₂ as the carrier gas, whereas CO₂, N₂, O₂ and CH₄ were quantified using a TCD with He as the carrier gas. Relative concentrations were calculated after the chromatographic response had been calibrated in partial pressure for each compound using "Air Liquide TM" and "Saphir". These standards are quality gas mixtures that include H₂, He, N₂, CO₂, O₂, CH₄, C₂H₆, C₃H₈, n-C₄H₁₀ and i-C₄H₁₀, available in the laboratory at different concentrations bracketing the samples' composition range. Each sample analysis was followed by a blank analysis to ensure the absence of carry over. Results are given with a precision of ± 5 vol.% for O₂, ±1.3 vol.% for CO₂, ±3 vol.% for N₂ and ±0.1 vol.% for CH₄ based on replicate measurements of gas standards of similar concentrations.

Water composition

All chemical analyses were carried out in the Total laboratories (Pau, CSTJF, France) using ion chromatography (Cl, Br and SO₄), Inductively Coupled Plasma-Atomic Emission Spectroscopy (Li, B and Sr), Inductively Coupled Plasma-Mass Spectrometry (Ca and Mg), and Flame Emission Spectrometry (Na, K, Ca and SiO₂). Accuracy for major elements was better than ± 5% and verified by repeated measurements of certified standard materials, namely Ion96-3 and LGC6020 (river waters) for cations and anions, and diluted Li and B ICP-AES standard solutions (Merck). Saline samples were analyzed either after dilution (to minimize matrix effects during measurement) or by adding a standard (to match the matrix of the standard materials). The matrix effects were validated on at least three dilutions (500, 1000, 2000).

3.3 Analytical methods – Isotopic compositions

CO₂ gas

The isotopic composition of the CO₂ gas was measured in Exetainer® vials at the IFPEN laboratory using a MAT253 (Finnigan Mat-Thermo Fisher) triple collection mass

spectrometer coupled to a gas chromatograph, operating with He as a carrier gas. An internal reference CO₂ gas was calibrated with the international gas reference standards RM8562, RM8563 and RM8564 with $\delta^{13}\text{C}_{\text{VPDB}}$ of $-3.76 \pm 0.03 \text{ ‰}$, $-41.56 \pm 0.04 \text{ ‰}$ and $-10.45 \pm 0.03 \text{ ‰}$, respectively (Verkouteren and Klinedinst, 2004). All the isotopic compositions given in this study are reported in the usual δ -scale in ‰ according to $\delta_{\text{sample}} (\text{‰}) = \{(\text{R}_{\text{sample}}/\text{R}_{\text{standard}}) - 1\} \times 1000$, where R is the $^{13}\text{C}/^{12}\text{C}$ atomic ratio. The uncertainties on $\delta^{13}\text{C}$ values are better than $\pm 0.4 \text{ ‰}$ based on the external reproducibility of internal standards.

N₂ gas

The isotopic composition of N₂ in gas samples stored in Exetainer[®] vials or stainless-steel cylinders was measured at the Institut de physique du globe de Paris (IPGP, France). The N₂ was purified and isolated from other gases before being transferred to the IRMS dual-inlet mass spectrometer Delta + XP (Finnigan Mat-Thermo Fisher) for isotopic analyses. N₂ purification was performed using the high vacuum line ($P < 10^{-5}$ mbar) described in Li et al. (2009) (details in Appendix). We obtained a relative uncertainty on the $\delta^{15}\text{N}$ better than $\pm 0.5 \text{ ‰}$ taking into account the N₂ extraction process efficiency and the reproducibility on an internal reference N₂ gas, itself calibrated against the air, the international reference standard for $\delta^{15}\text{N}$ measurements.

Noble gases

Noble gas isotopic compositions were measured at IPGP using the Helix-SFT (Split Flight Tube, Thermo Instruments[®]) following the protocol of Moreira et al. (2018) (details in Appendix). For Ne and Ar, the standard is the atmosphere. The helium standard is a gas collected at the Irene thermal spring (Reunion island) with a $^3\text{He}/^4\text{He}$ value (R) of $12.56 \pm 0.05 \text{ R}_\text{A}$ (with R_A the $^3\text{He}/^4\text{He}$ value of the air 1.4×10^{-6}). For the present study, blank corrections were negligible. Final uncertainties for the isotopic ratios in samples are ± 0.1 for $\text{R}/\text{R}_\text{A}$, ± 0.06 for $^{20}\text{Ne}/^{22}\text{Ne}$, ± 0.0005 for $^{21}\text{Ne}/^{22}\text{Ne}$, ± 5 for $^{40}\text{Ar}/^{36}\text{Ar}$ and correspond to the error propagation of the measured uncertainty, the blank correction, and the correction for mass discrimination.

Water isotopes

Oxygen and hydrogen isotope measurements were performed at BRGM stable isotope laboratory by equilibrating during one night 1 mL of water with gas mixtures of H₂–He and CO₂–He respectively for $\delta^2\text{H}$ and $\delta^{18}\text{O}$, and using a Finnigan MAT 252 mass spectrometer (Assayag et al., 2008). The external precision was $\pm 0.1 \text{ ‰}$ for $\delta^{18}\text{O}$ and $\pm 0.8 \text{ ‰}$ for $\delta^2\text{H}$ vs. SMOW.

Chlorine

The chlorine stable isotope compositions were measured at the IPGP on gaseous CH₃Cl that was prepared and purified with the method described in Godon et al. (2004). The $\delta^{37}\text{Cl}$ measurements were then performed on the dual-inlet IRMS Delta + XP. They are reported in Table A4 with the conventional $\delta^{37}\text{Cl}$ notation in per mil variations relative to Standard Mean Ocean Chlorine (SMOC). In this study, the external reproducibility of the seawater standard was $0 \pm 0.04 \text{ ‰}$ (1s, $n = 18$) as routinely obtained at IPGP for more than two decades (Godon et al., 2004). Four pore fluid samples were measured twice. The mean difference between duplicates was 0.04 ‰ .

$\delta^7\text{Li}$ analysis

In water samples, lithium isotopic compositions were measured using a Neptune Multi Collector ICP-MS (Thermo Fisher Scientific) at BRGM stable isotope laboratory. $^7\text{Li}/^6\text{Li}$ ratios were normalized to the L-SVEC standard solution (NIST SRM 8545) following the standard-sample bracketing method (Millot et al., 2004). The uncertainties on $\delta^7\text{Li}$ values are better than $\pm 0.5\%$ (2σ) based on the external reproducibility using internal standards (seawater IRMM BCR-403 and basalt JB-2).

In volcanic rocks, Li was separated from the matrix by ion-exchange chromatography using the method described in detail by Dellinger et al. (2015). After digestion, a sample aliquot was loaded onto a column filled with AG50-X12 resin and the Li was eluted in HCl 0.2 N. The Li isotopic composition was measured by MC-ICP-MS Neptune (Thermo Scientific, Bremen) at IPGP using an APEX desolvating system and at typical Li concentrations of 20–30 ppb. Each sample was successively measured three times within a standard-sample bracketing (SSB) sequence, yielding five $\delta^7\text{Li}$ values from which an average value was derived. Data were corrected for the background intensities recorded before each bracketing standard and each sample. The intensity of the background was no more than 0.5–1% of the sample intensity. The overall reproducibility and accuracy of the procedure (including solid sample digestion and Li separation) was checked by measurement of the basalt reference material BHVO-2 ($\delta^7\text{Li} = 4.23 \pm 0.83\%$; Ryu et al., 2014). The external error (2σ) was better than 0.5%. Finally, the concentration of the total procedural blank (acid digestion and column chemistry) was assessed to be less than 0.05 ng, i.e., insignificant compared with the amount of Li in the samples.

$\delta^{11}\text{B}$ analysis

Boron isotopic compositions of water samples were determined on a Finnigan MAT 261 solid source mass spectrometer in a dynamic mode at BRGM stable isotope laboratory. For these samples, water volumes corresponding to a mass of 10 μg of B underwent a two-step chemical purification using Amberlite IRA-743 selective resin according to a method adapted from Gaillardet and Allègre (1995). The uncertainties on $\delta^{11}\text{B}$ values are better than $\pm 0.3\%$ (2σ) based on the external reproducibility on the internal standard NBS951 ($\delta^{11}\text{B} = 4.05398 \pm 0.00105\%$).

Rock samples were dissolved by alkali fusion and B was extracted following the procedure of Chetelat et al. (2009) (details in Appendix). Boron isotope ratios were determined by MC-ICP-MS with a direct injection nebulizer (d-DIHEN; Louvat et al., 2014a) at IPGP with a 2σ reproducibility between 0.05 and 0.3%. $^{11}\text{B}/^{10}\text{B}$ values are expressed relative to the boric acid standard NBS 951 (NIST).

$^{87}\text{Sr}/^{86}\text{Sr}$ measurement

For water samples, chemical purification of Sr ($\sim 3 \mu\text{g}$) was performed using an ion-exchange column (Sr-Spec) before mass analysis according to a method adapted from Pin and Bassin (1992) with total blank $< 1 \text{ ng}$ for the entire chemical procedure. After chemical separation, around 150 ng of Sr were loaded onto a tungsten filament with tantalum activator and analyzed with a Finnigan MAT 262 multi-collector mass spectrometer at BRGM's stable isotope laboratory. The $^{87}\text{Sr}/^{86}\text{Sr}$ values were normalized to the certified value of the NBS987 standard 0.710240. An average internal precision of $\pm 10 \text{ ppm}$ (2σ) was obtained and the reproducibility of the $^{87}\text{Sr}/^{86}\text{Sr}$ ratio measurements was verified by repeated analysis of the NBS987 standard ($^{87}\text{Sr}/^{86}\text{Sr} = 0.710243 \pm 10$, 2σ).

For volcanic rocks, after total evaporation of ~0.2 mL of rock sample digestion solutions, the remaining solid was retaken with 0.1 mL of HNO₃ 3N and loaded onto a Sr-SPEC (Eichrom) resin chromatography column to separate ca. 200 ng of Sr (Pin and Bassin, 1992). The Sr isotopic composition was measured by MC-ICP-MS at IPGP. The mass discrimination was corrected using the invariant ratio ⁸⁸Sr/⁸⁶Sr (0.1194). Accuracy and reproducibility were verified by repeated analysis of the NBS standard SRM 987 (⁸⁷Sr/⁸⁶Sr = 0.710250±0.0000025).

3.5 PHREEQC modeling

The PHREEQC software, version 3 (Parkhurst and Appelo, 2013) was applied to compute aqueous speciation and fluid-mineral equilibria using the “thermoddem v1.10 06jun2017” thermodynamic database (website <http://thermoddem.brgm.fr/>; Blanc et al., 2012).

4. Results

4.1 Gas molecular and noble gases composition

Table 1. Analytical results of the gas sampled in 2017. $\delta^{15}\text{N}$ and $\delta^{13}\text{C}$ values are averaged from multiple measurements (n=2-6) except for sample PG17_116, which was analyzed only once for $\delta^{15}\text{N}$ (details in Table A1). See text for calculations of atmospheric N₂ proportion, $\delta^{15}\text{N}$ correction from atmospheric contribution and modeling results.

Sample no.	PG17_100	PG17_112	PG17_116	PG17_117
Sample location	La Salsa	La Rumba	El Gigante	El Ojo Verde
Latitude (°S)	21.619349	21.638776	21.64819	21.651306
Longitude (°W)	67.848462	67.852883	67.848736	67.840695
Temperature (°C)	43.4	44.6	41.5	36.2
Major composition (vol.%)				
CO ₂	74.7	66.2	86.0	38.4
CH ₄	0.04	0.03	0.00	0.07
O ₂	3.36	2.01	1.63	4.76
N ₂	21.8	32.0	12.4	56.4
% N ₂ atm	57.3	23.4	49.1	31.5
Isotopic composition (‰)				
$\delta^{13}\text{C}$ (±0.1‰, 2σ)	-11.2	-11.2	-11.2	-11.0
$\delta^{15}\text{N}$ (±0.5‰, 2σ)	2.7	1.8	1.6	2.3
$\delta^{15}\text{N}_{\text{primary}}$	6.4	2.3	3.1	3.4
Noble gases (ppm)				
⁴ He	337	517	109	814
²⁰ Ne	0.56	1.50	0.43	2.03
³⁶ Ar	7.1	12.9	3.6	12.2
⁴⁰ Ar/ ³⁶ Ar	298	288	283	288
R _C /R _A	3.68	3.84	3.81	3.86
Mantle He (%)	45.4	47.3	47.1	47.6
CO ₂ / ³ He _{surface}	4.35*10 ⁸	2.42*10 ⁸	1.51*10 ⁹	8.85*10 ⁷
Modeling				
CO ₂ / ³ He _{before degassing}	1.2*10 ⁸	9.6*10 ⁸	2.9*10 ⁹	4.7*10 ⁸
CO ₂ exsolution (%)	36	23	49	17

Thermal spring gases are mainly composed of CO₂ (38.4 to 86 vol. %) and N₂ (12.4 to 56.4 vol. %) with minor amounts of O₂ (1.63 to 4.76 vol. %) and negligible traces of CH₄ (< 0.07 vol. %; Table 1). No H₂ and H₂S were detected. If we assume that O₂ is derived from atmospheric contamination during sampling or natural diffusion into the thermal spring, we obtain a contribution of associated atmospheric N₂ up to 57.3% of the total N₂ (Table 1). Abundances of the Atmosphere-Derived Noble Gases (ADNG: ²⁰Ne and ³⁶Ar) are depleted relative to air and follow the composition expected for an Air Saturated Water (ASW; Fig. 3). In contrast, ⁴He is found in high proportions, from 109 to 814 ppm, with a high ³He/⁴He value normalized to air (R_C/R_A) of 3.79 ± 0.08 (with (³He/⁴He)_{air} = 1.4x10⁻⁶; Table 1). This value indicates a high mantle contribution (Sano and Marty, 1995, see discussion).

4.2 Gas C and N isotope compositions

The CO₂ gas sampled from thermal springs shows homogeneous δ¹³C values with an average of -11.1 ± 0.1‰ (Table 1, A1). In contrast, the isotopic composition of N₂ (δ¹⁵N) is more variable and ranges between 1.6 and 2.7 ± 0.5‰. Nitrogen isotope measurements of sample PG17_112 were performed on gases sampled in both Exetainers® and stainless-steel tubes to ensure good reproducibility of the results, regardless of the container used (Table A1). Similar values were obtained with a deviation of ±0.3‰. Considering an atmospheric contamination of up to 57.3% for N₂, we can estimate the primary δ¹⁵N value by isotopic mass balance as follows:

$$\delta^{15}\text{N}_{\text{measured}} = \delta^{15}\text{N}_{\text{atm}} \cdot \%_{\text{atm}} + \delta^{15}\text{N}_{\text{primary}} \cdot (1 - \%_{\text{atm}})$$

With atmospheric contamination %_{atm} up to 0.57 and δ¹⁵N_{atm} = 0‰, a maximum δ¹⁵N_{primary} of 6.4‰ is obtained (Table 1). We thus consider the measured values as minimum values.

4.3 Isotopic composition of water

Table 2. Chemical and isotopic compositions of Laguna Pastos Grandes waters. NICB: Normalized Ionic Charge Balance.

Sample no.	PG17-117	PG17-112	PG17-100	PG1_1	MV_1	PGS_1	PG17_99	SP_3	LS_4
Sampling trip	2017	2017	2017	2016	2016	2016	2017	2016	2016
Name	El Ojo Verde spring	La Rumba spring	La Salsa spring	La Salsa spring	El Gigante spring	Piedmont spring	Stream	Stream	Lake brine
Lat. (°S)	21.651306	21.638776	21.619349	21.61934	21.64865	21.61996	21.60764	21.69665	21.69552
Lg. (°W)	67.840695	67.852883	67.848462	67.84842	67.84866	67.85628	67.75753	67.8098	67.80927
T (°C)	36.2	44.6	43.4	42.2	45.7	32.4	17.3	16.4	24.5
pH	6.41	5.99	6.90	6.42	6.20	6.35	9.15	7.99	7.39
Alkalinity on site				10.7	8.91	4.35		0.78	
Chemical composition (mM)									
Na	232	137	173	220	251	23.7	0.57	1.17	3924
K	12.9	8.7	12.5	13.4	16.6	1.8	0.14	0.36	131
Ca	10.9	6.5	10.1	11.4	12.8	0.7	0.17	0.37	59.7
Mg	5.8	2.8	5.2	5.4	6.0	0.4	0.13	0.18	54.6
Alkalinity	7.4	5.3	7.4	7.4	8.9	1.8	0.90	0.79	10.9
SO ₄	2.9	2.3	2.3	2.9	4.2	0.8	0.04	0.22	39.5
Cl	278	173	197	258	291	25.5	0.73	1.52	4375
Li	11.1	6.6	9.9	7.7	9.6	0.8	0.02	0.25	74.8
Sr	0.11	0.06	0.11	0.11	0.15	0.01	0.001	0.003	1.03
B	3.6	2.2	3.3	3.2	4.7	0.5	0.04	0.08	28.6

Br	0.073	0.046	0.069	0.060	0.070	0.006	0.006	0.006	0.426
SiO ₂ *	116	101	116	155	152	101	36	60	60
Salinity**	16.2	10.1	11.5	15.1	17.0	1.49	0.04	0.09	256
NICB (%)	-1.3	-7.5	6.9	0.7	2.2	-3.1	-26.4	3.0	-2.9
pCO ₂ (mbar)***	141	309	60.3	110.0	389.0	61.7	0.03	0.5	10.5
Isotopic compositions (‰ ±2s)									
δ ² H (±0.8)	-92.2	-96.7	-93.9	-93.8	-92.5	-104.2	-99.4	-104.7	7.6
δ ¹⁸ O _{H2O} (±0.1)	-11.4	-12.4	-11.8	-11.7	-11.4	-14.2	-13.1	-13.2	3.3
δ ⁷ Li	5.2 ±0.1	5.6 ±0.1	3.8 ±0.1	3.6 ±0.1	4.0 ±0.2	2.6 ±0.2	4.0 ±0.2	10.9 ±0.1	3.9 ±0.3
δ ¹¹ B	-4.4 ±0.1	-5.0 ±0.1	-4.9 ±0.2	-4.3 ±0.3	-6.7 ±0.3	-6.0 ±0.3		0.0 ±0.3	-7.2 ±0.3
⁸⁷ Sr/ ⁸⁶ Sr	0.708384	0.708412	0.708398	0.708396	0.708402	0.708354	0.707950	0.707646	0.708327
2Sm	0.000005	0.000006	0.000010	0.000007	0.000006	0.000006	0.000010	0.000007	0.000007

*mg/L; **g/L; ***calculated with PHREEQC based on water chemistry

Spring waters exhibit a narrow range of δ¹⁸O (-14.2 to -11.4‰) and δ²H (-104.2 to -92.2‰), slightly more enriched in ¹⁸O and ²H than streams (with δ¹⁸O ~ -13.2‰ and -104.7 < δ²H < -99.4‰; Fig. 4, Table 2). They are located on the regional Ground and Spring Water Line (LGSWL; δ²H = 7.99 x δ¹⁸O + 0.3; n = 44) established by Fritz et al. (1981) and Rissmann et al. (2015) to the right of the Local Meteoric Water Line (LMWL) defined for modern precipitation in the Chilean and Bolivian Altiplano at altitudes of 2800 to 5700 m (δ²H = 8.15 x δ¹⁸O + 15.3; Chaffaut et al., 1998). Streams and springs define a trend given by the following equation: δ²H = 4.29 x δ¹⁸O + 43.8 (R² = 95 %, n = 8; Fig. 4b) with δ¹⁸O and δ²H values more positive than rainfall collected at 4500 m during the wet season. Two snow samples collected during the dry season show more positive δ¹⁸O and δ²H values than rainfall and fall to the left of the LMWL trend (Table A2). The Piedmont thermal spring, located on the border of the laguna, is shifted from the other springs toward more negative δ¹⁸O and δ²H values. In the southeastern part of Laguna Pastos Grandes, the brine sampled from the lake (LS4 sample) is enriched in both ¹⁸O and ²H compared to the inlet waters and has even greater δ¹⁸O and δ²H values than other Andean salars (Fig. 4, Table A2).

4.4 Geothermometry

The thermal waters associated with gases reach the surface at up to 46 °C, which is among the highest temperatures recorded in the Altiplano salars (Risacher and Fritz, 1991; Spiro et al., 1997). Based on the concentrations of some soluble elements (Si, Na, K, Ca, Mg, Li) in the thermal springs, we calculated the maximum temperature of the fluids at depth using empirical, semi-empirical and experimental equilibrium relations between water and minerals in the geothermal reservoirs (Sanjuan et al., 2014 and references therein). We used several geothermometers including silica, Na-K-Ca, Na-Li, Li-Mg, Li isotopes, and Na-K (details in Appendix; Table A3). They yield equilibrium temperatures for spring waters reacting with rocks of a deep reservoir that are comprised between 149 ±11 °C and 325 ±21 °C. The lowest value, given by the silica geothermometer, is probably underestimated because of silica precipitation during thermal water cooling (Verma and Santoyo, 1997). The highest value, given by Na/Li geothermometers, is overestimated because Li concentrations in the fluids are higher than those used for calibrations (Sanjuan et al., 2014). We thus retain a range of temperature between 200 and 250 °C obtained using δ⁷Li (200 ±25 °C; Millot et al., 2010) and Na/K (228 ±9 °C and 205 ±12 °C; Verma and Santoyo, 1997; Santoyo and Diaz-Gonzalez, 2010) geothermometers, as the maximum temperature encountered by the water through the faults of the Pastos Grandes caldera.

4.5 Chemical composition of the water

As extensively demonstrated in previous papers (Roche et al., 1991; Moquet et al., 2011), we assumed the atmospheric contribution to groundwater chemistry as negligible in this region and did not correct the data from this contribution. Elemental concentrations reported in this study are represented and interpreted together with those from previous studies of Laguna Pastos Grandes (Ballivian and Risacher, 1981; Hurlbert and Chang, 1984; Risacher and Fritz, 1991; Jones and Renaut, 1994). Spring waters have higher salinity (~14 g/L) than streams (0.09 g/L) and homogeneous $\delta^{37}\text{Cl}$ values of $0.25 \pm 0.03\%$ ($n=12$; Table A4). The Piedmont spring is the only exception with a relatively low salinity of 1.9 g/L. The brines from the southeastern part of the laguna are more saline than the water sources (256 g/L; Table 2).

Most of the waters show charge balances better than $\pm 8\%$ (Table 2), which denote a negligible influence of potential organic charges to the ionic balance. Due to higher sensitivity of low concentration samples to analytical errors, one stream sample shows a charge balance of -26% corresponding to a low anion excess of 0.41 mM.

Sodium and chloride are the dominant ions in spring waters, with average concentrations of 173 and 203 mM, respectively. With a Ca:Mg molar ratio ranging from 1.9 to 2.4, spring waters are enriched in Ca relative to Mg. Hydrothermal springs show similar relative ion concentrations suggesting that a common origin and common processes constrained the chemistry of their major elements (Fig. 5a). Their Ca:alkalinity molar ratio is favorable to the precipitation of large amounts of calcite (with a ratio of almost one Ca for two C). Compared with the hydrothermal springs, the Piedmont spring is diluted by surface waters. As for the laguna brine, it presents relative ion concentrations similar to those of the hydrothermal springs but with lower alkalinity (Fig. 5b).

4.6 $\delta^7\text{Li}$, $\delta^{11}\text{B}$ and $^{87}\text{Sr}/^{86}\text{Sr}$ in waters compared with surrounding rocks

Table 3. Chemical and isotopic data available for dacites, andesites and ignimbrites from Laguna Pastos Grandes. Data in italic are from previous studies.

Rock type	Ca/Na	Mg/Na	Li (ppm) ± 0.3 1SD	$\delta^7\text{Li}$ (‰)	B (ppm) ± 0.3 1SD	$\delta^{11}\text{B}$ (‰)	Sr (ppm) ± 3 1SD	$^{87}\text{Sr}/^{86}\text{Sr}$
Ignimbrite	0.61	0.30	66.9	-3.33 ± 0.47	54	-7.79 ± 0.21	330	0.725764
Dacite 1	0.70	0.45	147.4	-5.82 ± 0.12	60	-14.88 ± 0.21	351	0.707906
Dacite 2	0.87	0.36	80.2	-5.43 ± 0.35	30	-13.70 ± 0.15	464	0.706951
Andesite 1	1.69	1.50	279.7	-5.11 ± 0.38	144	-13.57 ± 0.09	690	0.705835
Andesite 2	2.13	1.61	147.8	-9.22 ± 0.15	116	-13.89 ± 0.10	706	0.706206
<i>Ignimbrite (Kaiser, 2014)</i>								0.708173
<i>Ignimbrite (Kaiser, 2014)</i>								0.708040
<i>Cenomanian-Turonian carbonates (McArthur et al., 1994)</i>								0.707298-0.707428
<i>Modern marine evaporites (Pierret et al., 2001)</i>								0.708940

Thermal springs show homogeneous $^{87}\text{Sr}/^{86}\text{Sr}$ values slightly more radiogenic than cold streams with average values of 0.70839 ± 0.00002 and 0.70780 ± 0.00021 , respectively. In

the eastern part of the laguna, the perennial lake has a $^{87}\text{Sr}/^{86}\text{Sr}$ value of 0.70833, slightly lower than thermal spring water values. As expected, all waters are within the range reported for dacites (0.70890 ± 0.00238 ; Cortecchi et al., 2005) and andesites (0.70763 ± 0.00161 ; Cortecchi et al., 2005) of the Andean Central Volcanic Zone. Our dataset is also compared with andesites, dacites and rhyolitic ignimbrites sampled in the vicinity of Laguna Pastos Grandes (Table 3). Sr isotope ratios of streams are between those of Pastos Grandes ignimbrites and dacites, whereas springs and brines show compositions similar to ignimbrites (Fig. 6a). The $^{87}\text{Sr}/^{86}\text{Sr}$ value of Cenomanian-Turonian marine carbonates, considered as the last open marine period in the central Andes (Deconinck et al., 2000), is much lower than the values of the thermal springs (with $^{87}\text{Sr}/^{86}\text{Sr} = 0.7073$ – 0.7074 ; McArthur et al., 1994).

Boron and lithium isotopic compositions of Pastos Grandes waters are also clearly different from seawater composition ($\delta^{11}\text{B} = 39.6\text{‰}$ and $\delta^7\text{Li} = 31.0\text{‰}$; Boschetti et al., 2017). $\delta^{11}\text{B}$ and $\delta^7\text{Li}$ values increase between rock and water samples in the following order: volcanic rocks < hydrothermal springs = lake brines < surface runoff. Pastos Grandes' thermal waters and brine present $\delta^{11}\text{B}$ and $\delta^7\text{Li}$ values around $-5.5 \pm 1.1\text{‰}$ and $+4.1 \pm 1.0\text{‰}$, respectively (Fig. 6b). In comparison, one stream displays more positive values for both $\delta^{11}\text{B}$ and $\delta^7\text{Li}$, at 0 and 10.9‰, respectively, whereas surrounding volcanic rocks are more negative, with $\delta^{11}\text{B}$ between -14.9 and -7.8‰ and $\delta^7\text{Li}$ between -9.2 and -3.3‰ (Fig. 6b; Table 3). In the study area, volcanic rocks have high Li and B concentrations (67–280 ppm of Li and 30–144 ppm of B) and isotopic compositions depleted in ^7Li and ^{11}B compared to the range of values for the Andean volcanic arc: 3–9 ppm of Li with $-6.4 < \delta^7\text{Li} < -4.5\text{‰}$ (Chan et al., 2002) and 6–60 ppm of B with $-7 < \delta^{11}\text{B} < +4\text{‰}$ (Rosner et al., 2003). Boron isotopic compositions of Pastos Grandes volcanic rocks are slightly higher than the average continental crust, estimated by Chaussidon and Albarède (1992) between -15 and -10‰.

4.7 Thermodynamic model

We compared the average spring water composition and the water chemistry obtained using PHREEQC modeling of volcanic bedrock alteration at 200–250 °C and CO_2 partial pressure varying between 10 and 100 bar (typical of CO_2 -rich geothermal systems; Lowenstern, 2001). The objective was to determine if the observed concentrations of major cations (Ca, Mg, K, Na and Si) can be reached by dissolution of the volcanic rocks (Table A5, see Appendix for the PHREEQC model) without input of ancient marine sediments. The mineralogy of the volcanic rocks surrounding Laguna Pastos Grandes was modeled with the following suite of minerals from the Thermoddem database (details in Appendix):

- Albite for the source of Na
- Anorthite for Ca
- Pargasite for Mg
- Quartz for Si
- Sanidine for K

In all models tested, the Si and DIC are higher than in the spring water. Ca, Mg, K and Na concentrations are best reproduced at 225 °C and 20 bar of CO_2 ($\text{SI}=1.3$; Fig. A2). To adjust the Cl concentration in the water, we tried different Cl sources: pure magmatic $\text{Cl}_2(\text{g})$ or halite. Modeling results were inconclusive with pure magmatic $\text{Cl}_2(\text{g})$ but consistent with halite, suggesting that the salinity of the spring water is provided by halite dissolution. As halite is commonly associated with gypsum in the sedimentary series of the Andean region, we also added anhydrite to the bedrock composition in the model. Despite this, the

main source of Ca in the spring waters remains anorthite (Table A5). All minerals were considered in the calculation as infinite reservoirs, except halite, which was fixed by the average Cl concentration in the spring water (239 mM).

5. Discussion

Laguna Pastos Grandes is a calcic-type salar characterized by Na-Ca-Cl brines that can, according to thermodynamic models, lead to the precipitation of calcite, the first mineral of the evaporation pathway before gypsum and ulexite (Hardie and Eugster, 1970; Risacher and Fritz, 2009). Although 19% of the salars in Bolivia (n=6) and 24% in Chile (n=12, Table A6) are calcic-type salars, massive calcite precipitation is only observed in Laguna Pastos Grandes. Gypsum, mirabilite (Na₂SO₄), halite and ulexite dominate the other calcic salars. This means that, in addition to the Ca²⁺ concentration, at least one parameter varies among the Andean salars and controls the magnitude of calcite precipitation in Laguna Pastos Grandes. The precipitation of carbonate minerals is complicated by biomineralization processes (mediated here by microorganisms; Jones and Renaut, 1994) and reaction kinetics in a near-surface continental environment (with ionic interactions, variable substrates, fluctuating pH, organic molecules and gas-phase interactions; Alonso-Zarza and Tanner, 2010). Still, the fundamental reasons why calcite precipitates in significant amounts are that i) Ca²⁺_(aq) and CO₃²⁻_(aq) are supplied in sufficient concentrations by water inputs and ii) surface processes allow the pH to increase, thereby dynamically sustaining supersaturation relative to calcite. At Laguna Pastos Grandes, we expect these processes to be related to dissolved CO₂ losses, such as degassing, salting-out by evaporation and photosynthesis. Our investigations therefore focused on the origin of CO₂ and Ca enrichment in water inputs.

5.1 Origin of CO₂ and N₂ in thermal spring gases

The thermal springs of Laguna Pastos Grandes discharge not only thermal waters but also gases that are essentially mixtures of CO₂ and N₂ (Table 1). This is common in the Central Andes (Spiro et al., 1997). Changes in the relative proportions of CO₂ and N₂ gases between sources in Laguna Pastos Grandes can be partly attributed to changes in the contribution from Air Saturated Waters (ASW) to the hydrothermal system. Indeed, the ⁴⁰Ar/³⁶Ar mean value of 289 in thermal springs is close to the air value of 295 (Nier, 1950) and their Atmosphere-Derived Noble Gases abundances (ADNG: ²⁰Ne and ³⁶Ar) normalized to air indicate that the atmospheric component in thermal springs (including O₂ and the atmospheric proportion of N₂) derives from ASW and not from air-contamination during sampling (Fig. 3).

Despite the ASW component, the mean R_C/R_A value of 3.79 ± 0.08 (Fig. 3, Table 1) indicates the presence of mantle-derived helium in the ascending hydrothermal gas. Our helium isotope results complement and confirm previous data from the central Andes, including an isolated analysis at Laguna Pastos Grandes (Fig. A3; Hilton et al., 1993; Hoke et al., 1994). Assuming that pure mantle-derived helium is characterized by R_C/R_A ~8, we calculated that about 47 % of the helium in Laguna Pastos Grandes is of mantle origin (using the calculations described in Hoke et al., 1994; Table 1), whereas it does not exceed 20% in other gas sources on the Altiplano. In the Western Cordillera, however, the supply of mantle helium reaches 69% at the Isluga volcano in Chile, 300 km north of Laguna Pastos Grandes (Hoke et al., 1994). In addition, the highest temperature of salar springs on

the Altiplano was recorded at Laguna Pastos Grandes, at 75 °C by Jones and Renaut (1994) and at 46 °C in this study (Table A6). For comparison, the maximum temperature recorded in the Western Cordillera is about 87 °C (Puchuldiza salar, northern Chile; Risacher et al., 2011). Therefore, the strong mantle influence in Laguna Pastos Grandes is probably due to its proximity to the active volcanic arc of the Western Cordillera (Table A6; Springer and Förster, 1998).

The average $\delta^{13}\text{C}$ value of $\text{CO}_2 \sim -11.1 \pm 0.1\text{‰}$ is lower than the typical value of a magmatic mantle-derived CO_2 source (between -9 and -4‰; Hoefs, 1980) that would be expected based on He results. Two hypotheses can be proposed to explain this low value: a contribution of CO_2 from sedimentary sources, i.e., organic carbon with $\delta^{13}\text{C} < -20\text{‰}$ (Hoefs, 1980), or carbonate precipitation during fluid ascent. To trace the origin of the CO_2 , $\delta^{13}\text{C}$ values are generally interpreted in relation to $\text{CO}_2/{}^3\text{He}$ values (Sano and Marty, 1995). In order to avoid the effects of hydrothermal degassing and liquid-vapor partitioning that could have significantly affected the $\delta^{13}\text{C}$ and $\text{CO}_2/{}^3\text{He}$ values of the gas, we determined the $\text{CO}_2/{}^3\text{He}$ composition at threshold P-T degassing conditions, using fluid phase equilibrium calculations applied to our system ($\text{H}_2\text{O}-\text{NaCl}-\text{CO}_2-\text{N}_2-\text{O}_2-\text{He}-\text{Ne}-\text{Ar}$; Rouchon et al., 2016). We assumed that all gaseous CO_2 was exsolved at a single supersaturation depth and that there was no carbonate precipitation (which would decrease the $\text{CO}_2/{}^3\text{He}$ value). The best results were obtained with an initial meteoric water recharge at high altitude, i.e. 5500 m, and a temperature of 0 °C. This is consistent with the $\delta^{18}\text{O}$ and $\delta^2\text{H}$ relationship in the spring waters, which suggests that the geothermal reservoir is fed during the wet season by meteoric water of rainfall isotopic composition (i.e., $\delta^{18}\text{O}$ of -16‰ and $\delta^2\text{H}$ of -123‰; Fig. 4 and Table A2 for values). Snow deposited during the dry season has different isotopic compositions (minimum $\delta^{18}\text{O}$ of -6.8‰ and $\delta^2\text{H}$ of -30.3‰). Considering a local geotherm of 45 °C/km (Rothstein and Manning, 2003), we calculated between 17 and 49% CO_2 exsolution at a depth of about 25-35 m (at 2.5-3.5 bar) in the different springs (Table 1). Before degassing, the $\text{CO}_2/{}^3\text{He}$ values were higher than those measured at the surface and ranged from $4.7 \cdot 10^8$ to $2.9 \cdot 10^9$. These values are in the range or slightly lower than the mantle value of $2 \cdot 10^9$ (Marty and Jambon, 1987). The depletion of CO_2 relative to ${}^3\text{He}$ in fluids could be consistent with carbonate precipitation during the geothermal fluid ascent. Since carbonates are enriched in ${}^{13}\text{C}$ relative to original CO_2 , this would also explain why the remaining CO_2 in the gas is depleted in ${}^{13}\text{C}$ (Ray et al., 2009).

Even so, we cannot completely rule out a minor contribution from thermal or microbial decomposition of organic matter in the underlying but unknown sedimentary rocks, perhaps accompanied to some extent by carbonate dissolution, which could account for the slight shift towards negative $\delta^{13}\text{C}_{\text{CO}_2}$ values relative to the mantle. Likewise, the $\delta^{15}\text{N}$ values between 2.3 and 6.4‰ could reflect a crustal (mean $\delta^{15}\text{N} = +7\text{‰}$; e.g. Sano et al., 1998) contribution mainly generated by biological or thermal degradation (Boyd, 2001). Although stratovolcanoes and their products dominate the South Lipez landscape of the Altiplano (e.g. de Silva and Francis, 1991), volcanic rocks probably overlain (Ludington et al., 1975) or incorporated (Risacher and Alonso, 2001) Cretaceous and Early Tertiary clastic to evaporitic sediments. Alternatively, as this region is close to the subduction zone of the Nazca plate under the South American plate (the slab being located at a depth of ~150-km below the Altiplano; Hoke et al., 1994; Kay and Coira, 2009), organic carbon and nitrogen could be remobilized from the slab by metamorphism (Gorman et al., 2006) and transported through primary melts into crustal intrusions. This hypothesis is supported by

the high Li concentrations and light $\delta^7\text{Li}$ recorded in volcanic lava flows surrounding Laguna Pastos Grandes (compared with MORB composition representing the upper mantle, $\delta^7\text{Li} = 3.7\text{‰}$; Misra and Froelich, 2012). It can only be interpreted as the addition of highly-negative $\delta^7\text{Li}$ slab-derived fluids to the mantle wedge beneath our study area (Fig. 7; Chan et al., 2002). Boron is also highly concentrated in the volcanic rocks of the area (30-144 ppm) and could come from the same source as Li. However, $\delta^{11}\text{B}$ values, between -14 and -8‰, are more negative than the lowest value of the slab-derived fluids predicted for the Andes (-2.8‰; Rosner et al., 2003). Boron is more volatile than lithium, and light $\delta^{11}\text{B}$ values are commonly observed in magmatic rocks (Chaussidon and Albarède, 1992) due to magma degassing effects, which produce ^{11}B depletion in the residual melt (Jiang and Palmer, 1998).

5.2 Hydrological history of spring water

The spring waters in Andean salars have previously been suggested to originate from the recycling of lake brines that continuously infiltrate through their bottom sediments (Risacher and Fritz, 1991; Risacher et al., 2003; Risacher and Fritz, 2009). The origin (and evolution) of the spring waters in Laguna Pastos Grandes can be assessed using their water isotopic composition. Spring waters lie on the local Ground and Spring Water Line (LGSWL) with slightly more positive $\delta^{18}\text{O}$ and $\delta^2\text{H}$ values than the local rainfall (Fig. 4), indicating that hydrothermal springs are genetically linked to meteoric waters. The slight enrichment in both ^{18}O and ^2H relative to meteoric water may imply either evaporative enrichment prior to infiltration at high altitude (Bershaw et al., 2016) or vapor loss during the ascent of thermal fluids (Cortecchi et al., 2005). In comparison, the laguna brine is highly enriched in ^{18}O and ^2H , ruling out the hypothesis of a significant recharge of the springs by infiltration of the laguna brine. In addition, the Cl/Br values of spring waters cannot be explained by a dilution of recycled brines by mixing with groundwater or meteoric water (Fig. 5c). We thus suggest that the solutes in the spring waters more likely derive from the alteration of the bedrock minerals.

5.3 Volcanic bedrock alteration at high temperature and pCO_2

$\delta^7\text{Li}$ and Na/K geothermometers applied to spring waters indicate that the meteoric water reached a maximum temperature of 200-250 °C after infiltration. Due to the high mantle-derived CO_2 flux delivered in thermal springs, the estimated pCO_2 in these waters (between 3 and 389 mbar estimated by PHREEQC; Table 2) spans the range and even exceeds the pCO_2 in spring waters of the Altiplano and Western Cordillera at 40 – 120 and 10 – 340 mbar, respectively (Morteani et al., 2014). This CO_2 enrichment can acidify thermal waters to a pH ~5 favoring bedrock minerals dissolution and hence thermal waters enrichment in solutes, especially in Ca. To test this hypothesis, we performed a series of PHREEQC simulations to determine the water composition resulting from the alteration of the volcanic bedrock with possible evaporites (halite, gypsum and anhydrite) from a meteoric water at 200, 225 and 250 °C and varying CO_2 partial pressures and compared the results to the average spring water composition (Table A5; Fig. A2).

The best results for Ca, Mg and K concentrations in spring waters were obtained by alteration of volcanic minerals at a temperature of 225 °C and at 20 bar of CO_2 (Fig. A2). This amount of CO_2 is compatible with the proximity of an ancient pre-eruptive magma reservoir at a depth of ~3 km as proposed by de Silva and Kay (2018). Under these

conditions, the main source of Ca in the water is the dissolution of Ca-rich feldspars rather than anhydrite (Table A5). These results are corroborated by Sr isotope data, which suggest that local meteoric waters interact with the host volcanic rocks (dacite, andesite and rhyolitic ignimbrite) rather than with ancient marine carbonates (Fig. 6a). Similarly, the $\delta^7\text{Li}$ and $\delta^{11}\text{B}$ values of the thermal waters and laguna brine are closer to those of the surrounding volcanic rocks than to those of seawater (Fig. 6b). $\delta^7\text{Li}$ values measured in waters are on average 8‰ higher than those measured in the surrounding rocks. This fractionation corresponds to the equilibrium isotopic fractionation between water and weathered volcanic rocks at high temperature ($200\pm 25^\circ\text{C}$; Millot et al., 2010). On the other hand, the average 7‰ positive $\delta^{11}\text{B}$ shift between springs and volcanic rocks can be explained either by adsorption of B on mineral surfaces during the ascent and cooling of hydrothermal fluid to the spring vent (Louvart et al., 2014b) or by the preferential incorporation of light B during carbonate precipitation (Vengosh et al., 1991).

Interestingly, the hydrothermal fluid obtained with these simulations is over-saturated with several carbonate minerals ($\text{SI}_{\text{calcite}}=1.23$, $\text{SI}_{\text{dolomite}}=3.03$, $\text{SI}_{\text{magnesite}}=2.02$), which supports the hypothesis (based on $\text{CO}_2/{}^3\text{He}$ and $\delta^{13}\text{C}$ data) that carbonate could have precipitated during fluid ascent. The higher Si concentration obtained in our simulations compared with those measured in spring waters together with the low temperature given by the SiO_2 geothermometer are also consistent with the precipitation of silica during fluid ascent. Furthermore, the simulations suggest that the salinity of the spring water most likely results from the dissolution of halite deposits. This interpretation is confirmed by the homogeneous $\delta^{37}\text{Cl}$ mean value of the springs at $0.25\pm 0.03\text{‰}$ ($n=12$; Table A4), as expected for halite precipitation in equilibrium with seawater at 25°C ($\delta^{37}\text{Cl} = 0.30 \text{‰}$; Eggenkamp et al., 2016). It indicates that over time, multiple cycles of halite precipitation and dissolution without new Cl inputs to the laguna have homogenized the Cl isotopic composition of the laguna brine and salts. Therefore, we can assume that Na and Cl originate from marine evaporites deposited during the last Cenomanian-Turonian marine period and later remobilized in Cretaceous and Tertiary continental deposits (Deconinck et al., 2000) that could have been either overlain by volcanic rocks or incorporated by volcanic eruptions as suggested by Risacher and Alonso (2001) for gypsum. This is also consistent with equimolar Cl and Na concentrations of these waters, typical of halite leaching (Fig. A4).

5.4 How is Laguna Pastos Grandes unique?

Ca:alkalinity molar ratios of waters of Laguna Pastos Grandes show that stream waters and mixed sources (Piedmont) are too diluted to contribute significantly to the growth of the carbonate platform. They also show that the laguna brine, which largely derives from spring waters (as suggested by chemical and isotopic data; Figs. 4, 5, 6), has been depleted in carbonate relative to Ca. Therefore, only the thermal springs have the potential to precipitate calcite massively (Fig. 5b). Most of the salars in the Central Andes are fed by thermal spring (60% in Bolivia and 78% in Chile) enriched in solutes compared with streams and regional groundwater (Table A6; Risacher and Fritz, 1991; Risacher et al., 2011). Modern carbonates are, however, absent or minor in these systems and generally precipitated as the first mineral of a more developed evaporitic sequence (Risacher and Fritz, 2009). Laguna Pastos Grandes is unique in this respect, as it hosts a $\sim 40 \text{ km}^2$ recent-to-modern carbonate platform spatially associated with thermal springs. There is a

remarkable mantle influence on these springs' temperature and gas composition, as well as on their solute enrichments (the highest of the Central Andes) with an average salinity of 14 g/l (Fig. 7; Table A6). This highlights the high water-rock reactivity of the hydrothermal system of Laguna Pastos Grandes compared to other salars, due to the high flow of CO₂ gas from the mantle. Furthermore, the singularity of this laguna is probably related to the mineralogy of the volcanic bedrock since calcic-type salars are limited to the Andean region. For example, Chilean volcanic rocks are known to be enriched in sulfides (Risacher and Alonso, 2001) and could be responsible for the greater abundance of sulfate-type salars (65%) compared to calcic-type salars.

6. Conclusion and perspectives

Bolivian and Chilean salars belong to broadly the same climatic and geological environment (Risacher and Fritz, 2009). Nevertheless, they vary widely in terms of chemistry and salt types mostly as a result of local variations in their fluid sources. In this study, we have shown that the western part of Laguna Pastos Grandes, characterized by abundant carbonate deposits, is mainly fed by thermal spring water, with minor contributions from rainfall and surrounding streams. We demonstrated that these spring waters, over-saturated with calcite, have been enriched in calcium and carbonate alkalinity by the alteration of the volcanic bedrock under high CO₂ partial pressure and a temperature of 200-250°C. The magmatic CO₂ and the high heat flow that drive the fluid circulation to the surface are probably due to a shallow pre-eruptive magma chamber as proposed by de Silva et al. (2006) and de Silva and Kay (2018) (i.e. at a typical depth of ~5 km; Fig. 7). We propose that this doping in magmatic CO₂ and the mineralogy of the volcanic bedrock are the reason for the large volumes of carbonates compared to most other modern Andean salars.

This configuration is not exclusive to Laguna Pastos Grandes system and can be found in many continental extensional settings (e.g. in Afar) where we posit, by analogy, that the same mechanisms are involved in the genesis of continental carbonate deposits in volcanic provinces. As identified in this study, the main factors that favor a significant production of carbonates would be a deep source of CO₂ and a Ca-rich volcanic basement allowing the following processes to occur:

- i. Alteration of a sulfide-poor volcanic bedrock containing Ca-enriched minerals (usually feldspars) at high pCO₂ (20 bar) and high temperature (225°C), leading to cationic enrichment of the waters and yielding calcic type hydrothermal waters.
- ii. At the surface, CO₂ degassing that leads to a pH increase and results in carbonate precipitation. CO₂ loss may also be driven by photosynthesis.
- iii. High evaporation rates, increasing both the solute concentrations above calcite saturation and the associated CO₂ salting-out, and resulting in a pH increase.

Laguna Pastos Grandes is therefore a unique natural laboratory that hosts a great diversity of carbonate facies (including pisoliths, ooids, muds and microbialites; Risacher and Eugster, 1979; Jones and Renaut, 1994; Bougeault et al., 2019), sometimes remarkably similar to ancient equivalents such as Cretaceous Presalt carbonates (Terra et al., 2010; Tosca and Wright, 2015). This laguna could, therefore, be further used to identify the biotic and/or abiotic controls involved in the formation of these carbonate deposits. Indeed, microbial mats and thin, dark, mucilaginous films locally coating the pool floors and pisolith surfaces in Laguna Pastos Grandes (described by Jones and Renaut, 1994 and

Bougeault et al., 2019) could also influence both the carbonate precipitation and fabrics (Pace et al., 2018; Gomez et al., 2018). Comprehensive geochemical, mineralogical and biodiversity studies are underway to characterize the links between physicochemical parameters, microbial communities and the diversity of carbonate fabrics observed in Laguna Pastos Grandes. These results will provide additional insight into the nature of the biosignatures preserved in microbialites's mineralogy and fabrics and allow us to further interpret the sedimentary record on our planet.

Acknowledgments, Samples, and Data

We would like to thank Total E&P Bolivia for field assistance (Serge Nicoletis, Jean-Pierre Meunier, Olivier-Daniel Moreau, Rozmarie Cuellar) and Total Lab (CSTJF, Pau, France; Carole Bortelle, Josiane Sentenac, Valérie Burg) for water analysis; Mathilde Mercuzot (Univ. Burgundy) for field and laboratory assistance (2016); Antoine Cogez for strontium isotopic analysis of volcanic rocks, Pierre Burckel for the chemical composition analysis of volcanic rocks, and BRGM (Catherine Guerrot team) for the chemical and isotopic measurements in water samples (2016). We would also like to thank Dr. Daniel Carrizo for providing the Chilean geological map. Particular thanks go to Magali Bonifacie for constructive discussion on chlorine isotope data. Funding was provided by Total EP R&D Carbonate Project (E. Poli). Parts of this work were supported by IPGP's multidisciplinary program PARI, and by the Paris-IdF region SESAME Grant no. 12015908. This is IPGP contribution No. 4062.

References

- Alonso-Zarza A. M. and Tanner L. H. (2010) Carbonates in continental settings: Facies, environments, and processes. *Dev. Sedim.* **61**, pp. 378.
- Assayag N., Jézéquel D., Ader M., Viollier E., Michard G., Prévot F., and Agrinier P. (2008) Hydrological budget, carbon sources and biogeochemical processes in Lac Pavin (France): constraints from $\delta^{18}\text{O}$ of water and $\delta^{13}\text{C}$ of dissolved inorganic carbon. *Appl. Geochem.* **23**(10), 2800-2816.
- Ballivian O. and Risacher F. (1981) Los salares del altiplano boliviano: métodos de estudio y estimación económica. IRD Editions.
- Bershaw J., Saylor J.E., Garzione C.N., Leier A. and Sundell K.E. (2016) Stable isotope variations ($\delta^{18}\text{O}$ and $\delta^2\text{H}$) in modern waters across the Andean Plateau. *Geochim. et Cosmochim. Acta* **194**, 310–324.
- Blanc P., Lassin A., Piantone P., Azaroual M., Jacquemet N., Fabbri A., and Gaucher E.C. (2012) Thermoddem: A geochemical database focused on low temperature water/rock interactions and waste materials. *Appl. Geochem.* **27**(10), 2107-2116.
- Boschetti T., Cortecchi G., Barbieri M. and Mussi M. (2007) New and past geochemical data on fresh to brine waters of the Salar de Atacama and Andean Altiplano, northern Chile. *Geofluids* **7**(1), 33-50.
- Boschetti T., Toscani L., Iacumin P. and Selmo E. (2017) Oxygen, Hydrogen, Boron and Lithium Isotope Data of a Natural Spring Water with an Extreme Composition: A Fluid from the Dehydrating Slab? *Aquat. Geochem.* **23**(5-6), 299-313.
- Bougeault C., Vennin E., Durlot C., Muller E., Mercuzot M., Chavez M., Gérard E., Ader M., Virgone A. and Gaucher E. C. (2019). Biotic–Abiotic Influences on Modern Ca–Si–Rich Hydrothermal Spring Mounds of the Pastos Grandes Volcanic Caldera (Bolivia). *Minerals* **9**(6), 380.
- Boyd S. R. (2001). Nitrogen in future biosphere studies. *Chem. Geol.* **176**(1-4), 1-30.

Chaffaut I., Coudrain-Ribstein A., Michelot J. L. and Pouyaud B. (1998) Précipitations d'altitude du Nord-Chili, origine des sources de vapeur et données isotopiques. *Bull. Inst. Fr. Etudes andines* **27**, 367-384 (in French).

Chan L.H., Edmond J.M., Thompson G. and Gillis K. (1992) Lithium isotopic composition of submarine basalts: implications for the lithium cycle in the oceans. *Earth Planet. Sci. Lett.* **108**, 151–160.

Chan L.H. and Kastner, M. (2000) Lithium isotopic composition of pore fluids and sediments in the Costa Rica subduction zone: implications for fluid processes and sediment contribution to arc volcanoes. *Earth Planet. Sci. Lett.* **183**, 275–290.

Chan L. H., Leeman W. P. and You C. F. (2002) Lithium isotopic composition of Central American volcanic arc lavas: implications for modification of subarc mantle by slab-derived fluids: correction. *Chem. Geol.* **182**(2-4), 293-300.

Chaussidon M. and Albarède F. (1992) Secular boron isotope variations in the continental crust: an ion microprobe study. *Earth Planet. Sci. Lett.* **108**(4), 229-241.

Chaussidon M. and Marty B. (1995) Primitive boron isotope composition of the mantle. *Science* **269**, 383–386.

Chetelat B., Liu C.-Q., Gaillardet J., Wang Q.L., Zhao Z.Q., Liang C.S., Xiao Y.K. (2009) Boron isotopes geochemistry of the Changjiang basin rivers. *Geochim. Cosmochim. Acta* **73**, 6084-6097.

Cortecchi G., Boschetti T., Mussi M., Lameli C. H., Mucchino C. and Barbieri M. (2005) New chemical and original isotopic data on waters from El Tatio geothermal field, northern Chile. *Geochim. J.* **39**(6), 547-571.

Deconinck J. F., Blanc-Valleron M. M., Rouchy J. M., Camoin G. and Badaut-Trauth D. (2000) Palaeoenvironmental and diagenetic control of the mineralogy of Upper Cretaceous–Lower Tertiary deposits of the Central Palaeo–Andean basin of Bolivia (Potosi area). *Sedim. Geol.* **132**(3-4), 263-278.

Dellinger M., Gaillardet J., Bouchez J., Calmels D., Louvat P., Dosseto A., Gorge C., Alanoca L. and Maurice L. (2015) Riverine Li isotope fractionation in the Amazon River basin controlled by the weathering regimes. *Geochim. Cosmochim. Acta* **164**, 71-93.

De Hoog J. C. and Savov I. P. (2018) Boron isotopes as a tracer of subduction zone processes. In *Boron Isotopes* (eds Springer, Cham), pp. 217-247.

de Silva S. L. and Francis P. W. (1991) Volcanoes of the Central Andes. Springer Verlag, Berlin.

de Silva S., Zandt G., Trumbull R., Viramonte J. G., Salas G. and Jimenez N. (2006) Large ignimbrite eruptions and volcano-tectonic depressions in the Central Andes: a thermomechanical perspective. In: Trois, C., De Natale, G., Kilburn, C.R.J. (Eds.), *Mechanism of Activity and Unrest at Large Calderas*, vol. 269. Geol. Soc. London, Spec. Publ., pp. 47-63.

de Silva S. and Kay S.M. (2018) Turning up the Heat: High-Flux Magmatism in the Central Andes. *Elements* **14**, 245-250.

Durand N., Monger H. C., Canti M. G. and Verrecchia E. P. (2018) Calcium carbonate features. In Interpretation of micromorphological features of soils and regoliths. Elsevier. pp. 205-258.

Eggenkamp H. G. M., Bonifacie M., Ader M., and Agrinier P. (2016) Experimental determination of stable chlorine and bromine isotope fractionation during precipitation of salt from a saturated solution. *Chem. Geol.* **433**, 46-56.

Fritz P., Suzuki O., Silva C. and Salati E. (1981) Isotope hydrology of groundwaters in the Pampa Del Tamarugal, Chile. *J. Hydrol.* **53**, 161–184.

Gaillardet J. and Allègre C. J. (1995) Boron isotopic compositions of corals: Seawater or diagenesis record? *Earth Planet. Sci. Lett.* **136**(3-4), 665-676.

Godon A., Jendryzejewski N., Eggenkamp H. G., Banks D. A., Ader M., Coleman M. L. and Pineau F. (2004) A cross-calibration of chlorine isotopic measurements and suitability of seawater as the international reference material. *Chem. Geol.* **207**(1-2), 1-12.

Gomez F. J., Kah L. C., Bartley J. K. and Astini R. A. (2014) Microbialites in a high-altitude Andean lake: multiple controls on carbonate precipitation and lamina accretion. *Palaios* **29**(6), 233-249.

Gomez F. J., Mlewski C., Boidi F. J., Farías M. E. and Gérard E. (2018) Calcium carbonate precipitation in diatom-rich microbial mats: the Laguna Negra hypersaline lake, Catamarca, Argentina. *J. Sedim. Res.* **88**(6), 727-742.

Gorman P. J., Kerrick D. M. and Connolly J. A. D. (2006) Modeling open system metamorphic decarbonation of subducting slabs. *Geochem. Geophys. Geosy.* **7**(4).

Gran, G. (1952). Determination of the equivalence point in potentiometric titrations. Part II. *Analyst* **77**(920), 661-671.

Hardie L. A. and Eugster H. P. (1970) The evolution of closed-basin brines. *Min. Soc. Am. Special Paper* **3**, 273-290.

Hilton D. R., Hammerschmidt K., Teufel S. and Friedrichsen H. (1993) Helium isotope characteristics of Andean geothermal fluids and lavas. *Earth Planet. Sci. Lett.* **120**(3-4), 265-282.

Hoefs J. (1980) *Stable isotope geochemistry*. Berlin and Heidelberg, Springer Verlag.

Hoke L., Hilton D. R., Lamb S. H., Hammerschmidt K. and Friedrichsen H. (1994) ³He evidence for a wide zone of active mantle melting beneath the Central Andes. *Earth Planet. Sci. Lett.* **128**(3-4), 341-355.

Hurlbert S. H. and Chang C. C. (1984) Ancient ice islands in salt lakes of the Central Andes. *Science* **224**(4646), 299-302.

Jiang S. Y. and Palmer M. R. (1998) Boron isotope systematics of tourmaline from granites and pegmatites; a synthesis. *Europ. J. Min.* **10**(6), 1253-1265.

Jones B. and Renaut R. W. (1994) Crystal fabrics and microbiota in large pisoliths from Laguna Pastos Grandes, Bolivia. *Sedimentology* **41**(6), 1171-1202.

Kaiser J. F. (2014) Understanding large resurgent calderas and associated magma systems: the Pastos Grandes Caldera Complex, southwest Bolivia. PhD thesis of Oregon State University.

Kay S. M. and Coira B. L. (2009) Shallowing and steepening subduction zones, continental lithospheric loss, magmatism, and crustal flow under the Central Andean Altiplano-Puna Plateau. *Backbone of the Americas: shallow subduction, plateau uplift, and ridge and terrane collision*, 204, 229.

Li L., Cartigny P. and Ader M. (2009) Kinetic nitrogen isotope fractionation associated with thermal decomposition of NH₃: Experimental results and potential applications to trace the origin of N₂ in natural gas and hydrothermal systems. *Geochim. Cosmochim. Acta* **73**(20), 6282-6297.

Louvat P., Moureau J., Paris G., Bouchez J., Noireaux J., Gaillardet J. (2014a) A fully automated direct injection nebulizer (d-DIHEN) for MC-ICP-MS isotope analysis: application to boron isotope ratio measurements. *J. Anal. Atom. Spectrom.* **29**(9), 1698-1707.

854 Louvat P., Gayer E. and Gaillardet J. (2014b) Boron behavior in the rivers of Réunion
 855 island, inferred from boron isotope ratios and concentrations of major and trace elements.
 856 *Proced. Earth Plan. Sci.* **10**, 231-237.
 857 Lowenstern J. B. (2001) Carbon dioxide in magmas and implications for hydrothermal
 858 systems. *Miner. Deposita* **36**(6), 490-502.
 859 Luddington S., Orris G.J., Cox D.P., Long K.R. and Asher-Bolinden S. (1975) Mineral
 860 deposit models. In *Geology and Mineral Resources of the Altiplano and the Cordillera*
 861 *Occidental, Bolivia* (eds Bleiwas D. J. and Christiansen R. G.). U.S. Geol. Survey Bull.
 862 pp. 63-224
 863 Luddington S., Orris G.J., Cox D.P., Long K.R. and Asher-Bolinder S. (1992) Mineral
 864 deposit models. In *Geology And Mineral Resources Of The Altiplano and Cordillera*
 865 *Occidental, Bolivia* (eds by U.S. Geological Survey and Servicio Geolbgico de Bolivia).
 866 Bull. US geol. Surv. 1975, pp. 63-89.
 867 Marschall H. R. (2018) Boron isotopes in the ocean floor realm and the mantle. In *Boron*
 868 *Isotopes* (eds Springer, Cham), pp. 189-215.
 869 Marty B. and Jambon A. (1987) ³He in volatile fluxes from the solid Earth: Implications
 870 for carbon geodynamics. *Earth Plan. Sci. Lett.* **83**, 16-26.
 871 McArthur J. M., Kennedy W. J., Chen M., Thirlwall M. F. and Gale A. S. (1994)
 872 Strontium isotope stratigraphy for Late Cretaceous time: direct numerical calibration of
 873 the Sr isotope curve based on the US Western Interior. *Palaeogeo. Palaeoclim.*
 874 *Palaeoeco.* **108**(1-2), 95-119.
 875 Millot R., Guerrot C. and Vigier N. (2004) Accurate and high-precision measurement of
 876 lithium isotopes in two reference materials by MC-ICP-MS. *Geostand. Geoanal. Res.*
 877 **28**(1), 153-159.
 878 Millot R., Scaillet B. and Sanjuan B. (2010) Lithium isotopes in island arc geothermal
 879 systems: Guadeloupe, Martinique (French West Indies) and experimental approach.
 880 *Geochim. Cosmochim. Acta* **74**, 1852-1871.
 881 Misra S. and Froelich P. N. (2012) Lithium isotope history of Cenozoic seawater:
 882 changes in silicate weathering and reverse weathering. *Science* **335**(6070), 818-823.
 883 Moquet J. S., Crave A., Viers J., Seyler P., Armijos E., Bourrel L., Chavarri E.N, Lagane
 884 C., Laraque A., Lavado Casimiro W.S., Pombosa R., Noriega L., Vera A. and Guyot J.L.
 885 (2011) Chemical weathering and atmospheric/soil CO₂ uptake in the Andean and
 886 Foreland Amazon basins. *Chem. Geol.* **287**(1-2), 1-26.
 887 Moreira M., Rouchon V., Muller E. and Noirez S. (2018) The xenon isotopic signature of
 888 the mantle beneath Massif Central. *Geochem. Perspect. Lett.* **6**, 28-32.
 889 Moriguti T. and Nakamura E. (1998) Across-arc variation of Li isotopes in lavas and
 890 implications for crust/mantle recycling at subduction zones. *Earth Planet. Sci. Lett.*
 891 **163**(1-4), 167-174.
 892 Morteani G., Möller P., Dulski P. and Preinfalk C. (2014) Major, trace element and stable
 893 isotope composition of water and muds precipitated from the hot springs of Bolivia: Are
 894 the waters of the spring's potential ore forming fluids? *Chemie der Erde-Geochemistry*
 895 **74**(1), 49-62.
 896 Nier A. O. (1950) A redetermination of the relative abundances of the isotopes of carbon,
 897 nitrogen, oxygen, argon and potassium. *Phys. Rev.* **77**(6), 789-793.
 898 Ozima M. and Podosek F. A. (2002) *Noble Gas Geochemistry*. Cambridge University
 899 Press.
 900 Pace A., Bourillot R., Bouton A., Vennin E., Braissant O., Dupraz C., Duteil T.,
 901 Bundeleva I., Patrier P., Galaup S., Yokoyama Y., Franceschi M., Virgone A. and

902 Visscher P.T. (2018) Formation of stromatolite lamina at the interface of oxygenic–
 903 anoxygenic photosynthesis. *Geobiology* **16**(4), 378-398.
 904 Parkhurst D.L. and Appelo C.A.J. (2013) Description of input and examples for
 905 PHREEQC version 3 – a computer program for speciation, batch-reaction, one-
 906 dimensional transport, and inverse geochemical calculations. U.S. geological survey
 907 techniques and methods, book 6, chap. A43, pp 497.
 908 Pierret M. C., Clauer N., Bosch D., Blanc G. and France-Lanord C. (2001). Chemical and
 909 isotopic ($^{87}\text{Sr}/^{86}\text{Sr}$, $\delta^{18}\text{O}$, δD) constraints to the formation processes of Red-Sea brines.
 910 *Geochim. Cosmochim. Acta* **65**(8), 1259-1275.
 911 Pin C. and Bassin C. (1992) Evaluation of a strontium-specific extraction
 912 chromatographic method for isotopic analysis in geological materials. *Analytica Chimica*
 913 *Acta* **269**(2), 249-255.
 914 Pineau F. and Javoy M. (1983) Carbon isotopes and concentrations in mid-Atlantic ridge
 915 basalts. *Earth Planet. Sci. Lett.* **29**, 413-421.
 916 Ray M.C., Hilton D.R., Muñoz J., Fischer T.P. and Shaw A.M. (2009) The effects of
 917 volatile recycling, degassing and crustal contamination on the helium and carbon
 918 geochemistry of hydrothermal fluids from the Southern Volcanic Zone of Chile. *Chem.*
 919 *Geol.* **266**(1-2), 38-49.
 920 Risacher F. and Eugster H. P. (1979) Holocene pisoliths and encrustations associated
 921 with spring-fed surface pools, Pastos Grandes, Bolivia. *Sedimentology* **26**(2), 253-270.
 922 Risacher F. and Fritz B. (1991) Geochemistry of Bolivian salars, Lipez, southern
 923 Altiplano: origin of solutes and brine evolution. *Geochim. Cosmochim. Acta* **55**(3), 687-
 924 705.
 925 Risacher F., and Alonso H. (2001) Geochemistry of ash leachates from the 1993 Lascar
 926 eruption, northern Chile. Implication for recycling of ancient evaporites. *J. volcano.*
 927 *geoth. Res.* **109**(4), 319-337.
 928 Risacher F. and Fritz B. (2009) Origin of salts and brine evolution of Bolivian and
 929 Chilean salars. *Aquat. Geochem.* **15**(1-2), 123-157.
 930 Risacher F., Alonso H. and Salazar C. (2003) The origin of brines and salts in Chilean
 931 salars: a hydrochemical review. *Earth-Sci. Rev.* **63**(3-4), 249-293.
 932 Risacher F., Fritz B. and Hauser A. (2011) Origin of components in Chilean thermal
 933 waters. *J. S. Am. Earth Sci.* **31**(1), 153-170.
 934 Rissmann C., Leybourne M., Benn C. and Christenson B. (2015) The origin of solutes
 935 within the groundwaters of a high Andean aquifer. *Chem. Geol.* **396**, 164-181.
 936 Roche M.A., Fernandez Jauregui C., Aliaga A., Bourges J., Cortes J., Guyot J.L., Pena J.
 937 and
 938 Rosner M., Erzinger J., Franz G. and Trumbull R.B. (2003) Slab- derived boron isotope
 939 signatures in arc volcanic rocks from the Central Andes and evidence for boron isotope
 940 fractionation during progressive slab dehydration. *Geochem. Geophys. Geosy.* **4**, 1–25.
 941 Rothstein D.A. and Manning C.E. (2003) Geothermal gradients in continental magmatic
 942 arcs: Constraints from the eastern Peninsular Ranges batholith, Baja California, México.
 943 In *Tectonic evolution of northwestern México and the southwestern USA: Boulder,*
 944 *Colorado* (eds. Johnson S.E. et al.) *Geological Society of America Special Paper* **374**, pp.
 945 337–354.
 946 Rouchon V., Courtial X., Durand I., Garcia B., Creon L. and Mougin P. (2016) A Fluid
 947 Phase

948 Equilibria Model in the System CO₂-N₂-H₂O-NaCl-He-Ne-Ar Below 200 Bar and 150°C
 949 – Application to CO₂/He Fractionation in Continental Mantle Degassing. Goldschmidt
 950 Abstracts 2658.
 951 Rounds S. A., and Wilde F. D. (2012) Chapter A6. Section 6.6. Alkalinity and acid
 952 neutralizing capacity. In US Geological Survey TWRI book 09.
 953 Ryu J. S., Vigier N., Lee S. W., Lee K. S. and Chadwick O. A. (2014) Variation of
 954 lithium isotope geochemistry during basalt weathering and secondary mineral
 955 transformations in Hawaii. *Geochim. Cosmochim. Acta* **145**, 103-115.
 956 Salisbury M. J., Jicha B. R., de Silva S. L., Singer B. S., Jiménez N. C., and Ort M. H.
 957 (2011) ⁴⁰Ar/³⁹Ar chronostratigraphy of Altiplano-Puna volcanic complex ignimbrites
 958 reveals the development of a major magmatic province. *Bulletin*, 123(5-6), 821-840.
 959 Sano Y. and Marty B. (1995) Origin of carbon in fumarolic gas from island arcs. *Chem.*
 960 *Geol.* **119**(1-4), 265-274.
 961 Sano Y., Takahata N., Nishio Y. and Marty B. (1998) Nitrogen recycling in subduction
 962 zones. *Geophy. Res. Lett.* **25**, 2289-2292.
 963 Santoyo E., and Díaz-González L. (2010) A new improved proposal of the Na/K
 964 geothermometer to estimate deep equilibrium temperatures and their uncertainties in
 965 geothermal systems. Proceedings World Geothermal Congress, Bali, Indonesia.
 966 Sanjuan B., Millot R., Ásmundsson R., Brach M. and Giroud N. (2014) Use of two new
 967 Na/Li geothermometric relationships for geothermal fluids in volcanic environments.
 968 *Chem. Geol.* **389**, 60-81.
 969 Spiro B., Hoke L. and Chenery C. (1997) Carbon-isotope characteristics of CO₂ and CH₄
 970 in geothermal springs from the Central Andes. *Internat. Geol. Rev.* **39**(10), 938-947.
 971 Springer M., and Förster, A. (1998). Heat-flow density across the central Andean
 972 subduction zone. *Tectonophysics* **291**, 123-139.
 973 Teboul P. A., Durllet C., Gaucher E. C., Virgone A., Girard J. P., Curie J., ... and Camoin
 974 G. F. (2016) Origins of elements building travertine and tufa: New perspectives provided
 975 by isotopic and geochemical tracers. *Sedim. Geol.* **334**, 97-114.
 976 Teboul P. A. (2017) Diagenesis of lower Cretaceous presalt continental carbonates from
 977 the West African margin: simulations and analogues (Doctoral dissertation, Aix-
 978 Marseille).
 979 Terra G.J.S., Spadini A.R., França A.B., Sombra C.L., Zambonato E.E., da Silva
 980 Juschaks L.C., Arienti L.M., Erthal M.M., Blauth M., Franco M.P., Matsuda N.S., da
 981 Silva N.G.C., Moretti Junior P.A., D'Avila R.S.F., de Souza R.S., Tonietto S.N., Couto
 982 dos Anjos S.M., Campinho V.S. and Winter W.R. (2010) Classificação de rochas
 983 carbonáticas aplicável às bacias sedimentares brasileiras. *Bulletin Geoscience Petrobras,*
 984 *Rio de Janeiro* **18** (1), 9–29
 985 Thorpe R. S., Potts P. J., and Francis P. W. (1976) Rare earth data and petrogenesis of
 986 andesite from the North Chilean Andes. *Contrib. Mineral. Petr.* **54**(1), 65-78.
 987 Tosca N.J., Wright V.P. (2015) Diagenetic pathways linked to labile Mg-clays in
 988 lacustrine carbonate reservoirs: a model for the origin of secondary porosity in the
 989 Cretaceous Pre-salt Barra Velha Formation, Offshore Brazil, 435. *Geological Society of*
 990 *London, Special Publication.* SP435-1.
 991 Vengosh A., Kolodny Y., Starinsky A., Chivas A. R. and McCulloch M. T. (1991)
 992 Coprecipitation and isotopic fractionation of boron in modern biogenic carbonates.
 993 *Geochim. Cosmochim. Acta* **55**(10), 2901-2910.

994 Verkouteren R. M. and Klinedinst D. B. (2004) Value Assignment and Uncertainty
 995 Estimation of Selected Light Stable Isotope Reference Materials: RMs 8543-8545, RMs
 996 8562-8564, and RM 8566. *NIST Special Publication* **260** (149), 59.
 997 Verma S. P. and Santoyo E. (1997) New improved equations for Na/K, Na/Li and SiO₂
 998 geothermometers by outlier detection and rejection. *J. Volcanol. Geoth. Res.* **79**(1-2), 9-
 999 23.
 1000 Verrecchia E.P. (2007) Lacustrine and palustrine geochemical sediments - Chapter 9. In:
 1001 *Terrestrial geochemical sediments and geomorphology* (Eds. D.J. Nash and S.J.
 1002 McLaren), Blackwell, London, Oxford, pp. 298-329.
 1003 Zamanian K., Pustovoytov K. and Kuzyakov Y. (2016). Pedogenic carbonates: Forms
 1004 and formation processes. *Earth-Sci. Rev.* **157**, 1-17.

Figure Captions

Fig. 1: **a.** Topographic map of the Central Andes showing the location of Laguna Pastos Grandes among the main Chilean and Bolivian salars (in white); **b.** Zoom on the geological context of Laguna Pastos Grandes (modified from Bougeault et al., 2019); satellite image provided by Zoom Earth website, © 2018 Microsoft Corporation Earthstar Geographics SIO; **c.** View of the carbonate platform with partially submerged calcitic pisoliths.

Fig. 2: Location of water and gas sampling in streams (blue stars), thermal springs (red stars) and brine in one of the sustainable lakes (yellow star) in Laguna Pastos Grandes (Bolivia). The location of the volcanic rock samples is also indicated by black dots. The four thermal springs (images 1-4) flow up through the recent carbonate platform developing to the west of the laguna. The arrows indicate gas bubbling in the water basins, except for "El Gigante" where gas and water have separate vents. Ign.: Ignimbrite; Dac.: Dacite; And.: Andesite.

Fig. 3: Relative abundance of air-normalized isotopic composition of noble gas (^4He , ^{20}Ne , ^{36}Ar , $^{40}\text{Ar}/^{36}\text{Ar}$ and $^3\text{He}/^4\text{He}$) in thermal springs El Ojo Verde, La Rumba, La Salsa and El Gigante. The normalization values used as references are 295.5 for $^{40}\text{Ar}/^{36}\text{Ar}$ ratio (Nier, 1950) and 1.39×10^{-6} for $^3\text{He}/^4\text{He}$ ratio (Ozima and Podosek, 2002). Helium isotope ratios are corrected for the effects of ASW (Air saturated Water) contamination in hydrothermal system and are equivalent to R_c/R_a .

Fig. 4: Plot of $\delta^{18}\text{O}$ versus $\delta^2\text{H}$ for Pastos Grandes waters. Plot b is focused on thermal springs (in red) and cold streams (in blue) compared to a rain sample (in white) collected at the same altitude during the wet season in March 2017. Two snow samples (grey) were also collected during the dry season in January 2016. Rainfall and snow data are presented in Table A2. The composition of the lake brine (in yellow) of Pastos Grandes is compared to other Andean salars (in black, based on this study and Boschetti et al., 2007; Table A2). The Local Meteoric Water Line (LMWL; Chaffaut et al., 1998) and the Local Ground- and Spring-Water Line (LGSWL; Rissmann et al., 2015) for the South-Central Andes are also indicated.

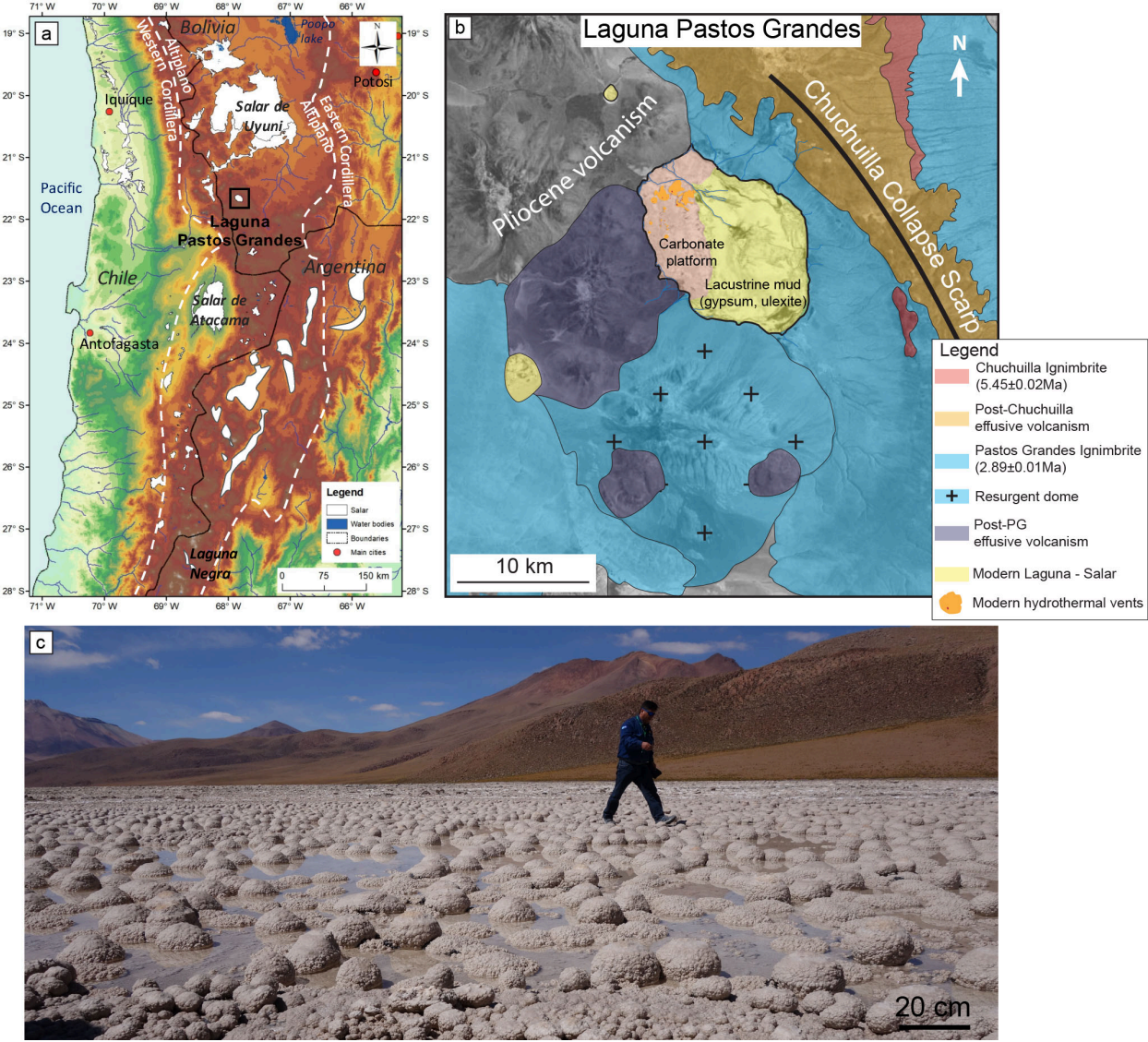
Fig. 5: Chemical composition of Laguna Pastos Grandes water sources (thermal springs in red/orange and streams in blue) and lake brine (in yellow). **a.** Schoeller diagram showing relative concentrations in solutes; **b.** Plot of Ca versus Alkalinity (mM); **c.** Plot of Cl concentration versus Cl/Br. Data from this study are presented as dots and previous data as squares (Ballivian and Risacher, 1981; Hurlbert and Chang, 1984; Risacher and Fritz, 1991; Jones and Renaut, 1994).

Fig. 6: Sr, Li and B isotopic compositions of Laguna Pastos Grandes water sources (thermal springs in red and streams in blue) and lake brine (in yellow) compared with andesite, dacite (this study), and rhyolitic ignimbrite (this study and Kaiser, 2014) from the Pastos Grandes caldera. **a.** $^{87}\text{Sr}/^{86}\text{Sr}$ vs Sr concentration (mg/l) data compared to Cenomanian-Turonian marine carbonates (McArthur et al., 1994) representing the last marine sedimentary sequence in the Central Andes region and modern marine evaporites (Pierret et al., 2001). Mean values of dacite (D) and andesite (A) from the Andean Central Volcanic Zone (CVZ) are also given for comparison (Cortecci et al., 2005); **b.** $\delta^{11}\text{B}$ vs $\delta^7\text{Li}$ data

1053 compared to modern seawater (Boschetti et al., 2017) and rocks from the Andean volcanic
1054 arc (Chan et al., 2002; Rosner et al., 2003).

1055
1056 Fig. 7: Conceptual model of modern carbonate precipitation in relation to water and gas
1057 sources in Laguna Pastos Grandes. Violet-blue arrows refer to hydrothermal circulations.
1058 See the conclusion for more details. Boron isotope data are from De Hoog and Savov
1059 (2018) for the Altered Oceanic Crust (AOC) and marine sediments and Marschall (2018)
1060 for the mantle. Lithium isotope data are from Chan and Kastner (2000) for subducted
1061 sediments, Moriguti and Nakamura (1998) and Chan et al. (1992) for AOC and Misra and
1062 Froelich (2012) for the mantle. Nitrogen isotope data are from Sano et al. (1998) for the
1063 crust. Carbon isotope data are from Hoefs (1980) for sedimentary organic carbon and
1064 Pineau and Javoy (1983) for mantle-derived signature. Rc/Ra data are from Hoke et al
1065 (1994). Other data are from this study.

1067 Figure 1



1068
1069

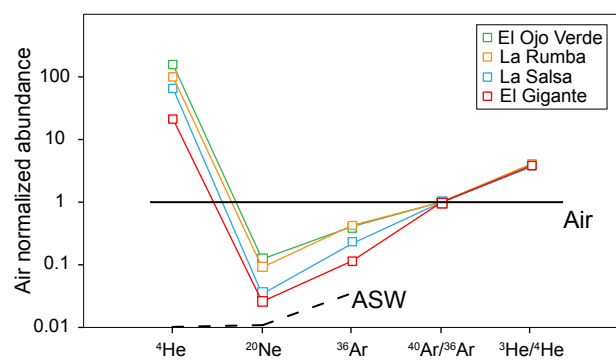
1070

Figure 2



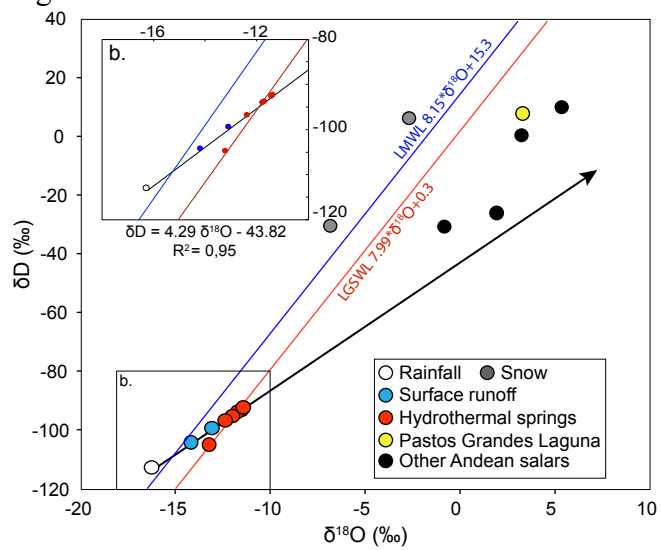
1071
1072

1073 Figure 3



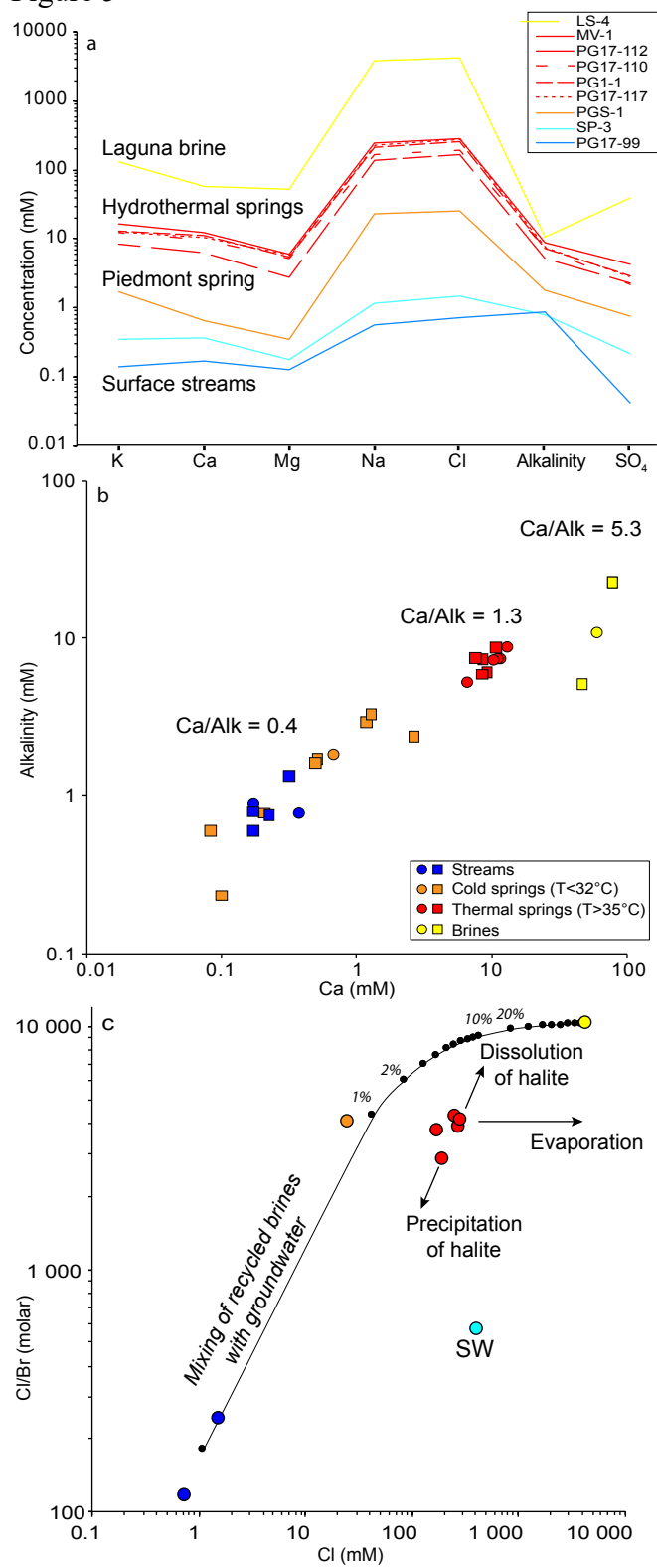
1074
1075

1076 Figure 4



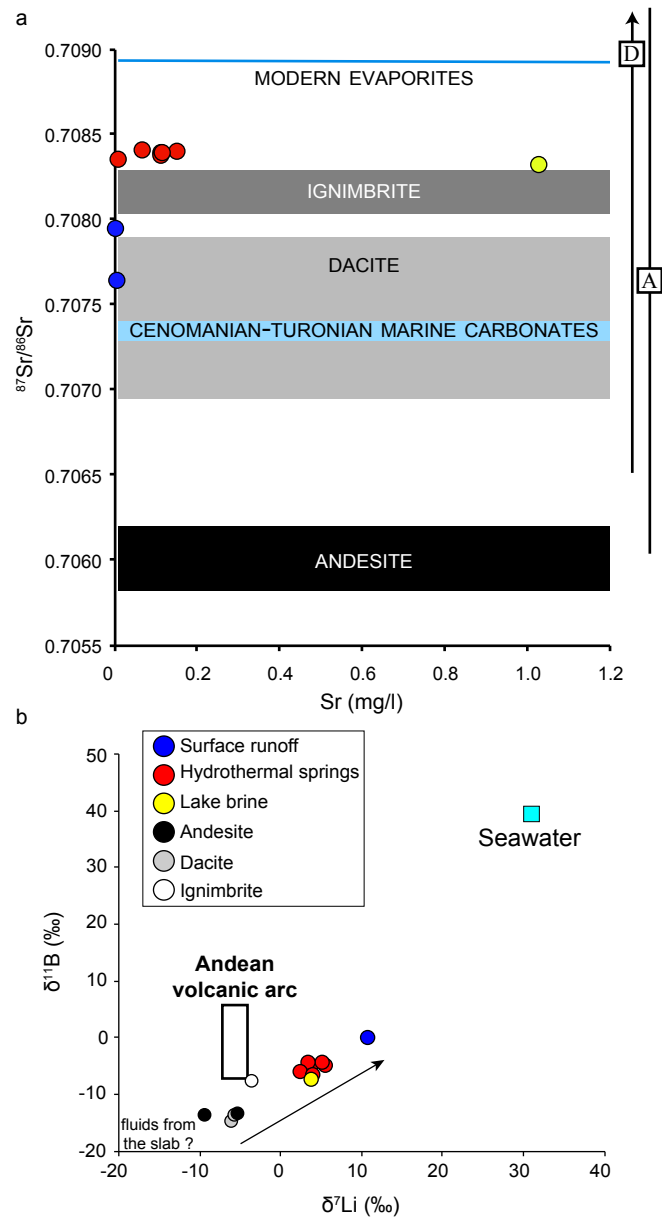
1077
1078

1079 Figure 5



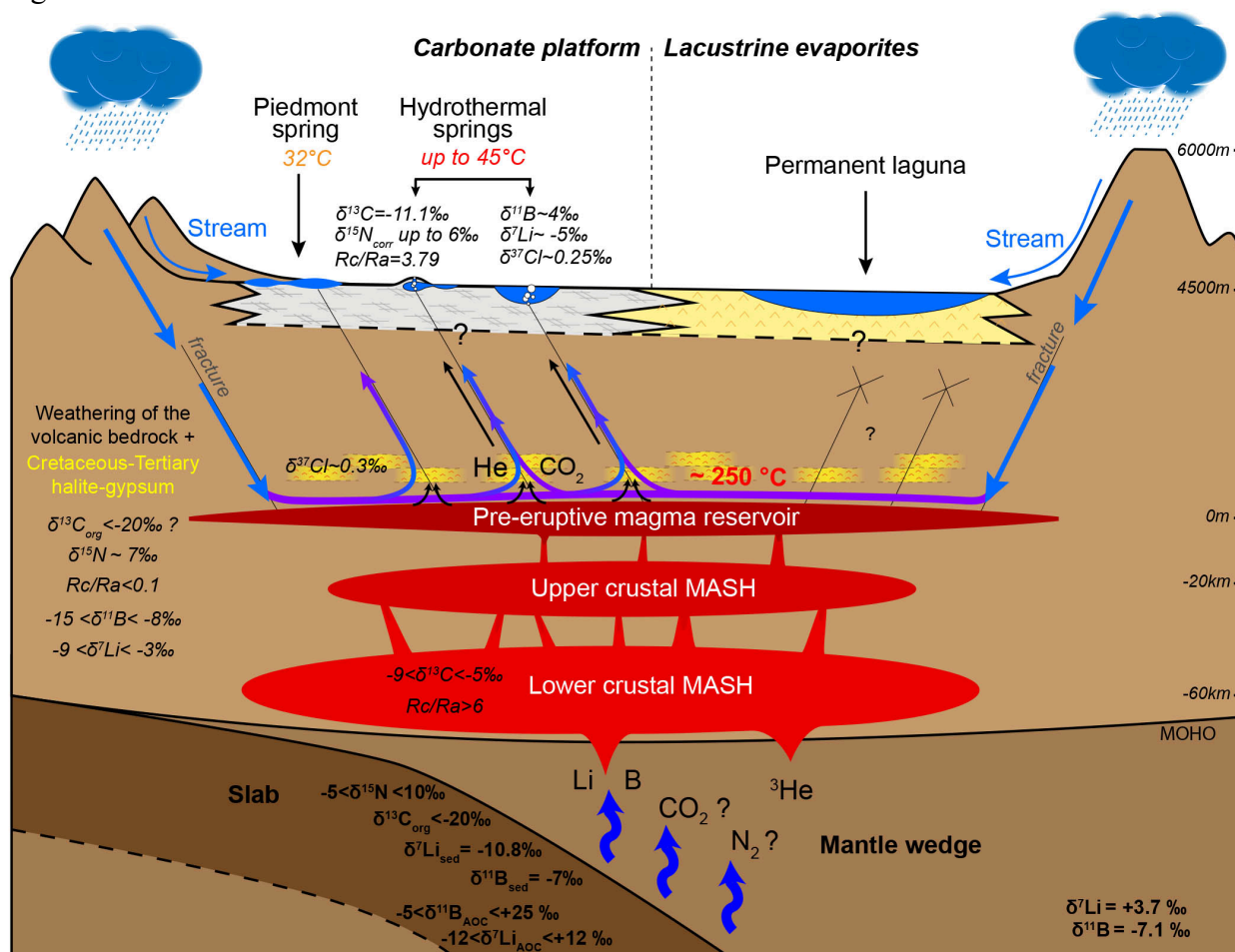
1080
1081

1082 Figure 6



1083
1084

1085 Figure 7



1086
1087

1088

Appendix of

1089

A Multi-Tracers Analysis of Gas and Solutes in Laguna Pastos Grandes (Bolivia): Key Proxies of the Origin of Continental Carbonates in Andean Salars

1090

1091

E. Muller¹, E. C. Gaucher², C. Durllet³, J.S. Moquet¹, M. Moreira¹, V. Rouchon⁴, P. Louvat¹, G. Bardoux¹, S. Noirez⁴, C. Bougeault³, E. Vennin³, E. Gérard¹, M. Chavez⁵, A. Virgone², M. Ader¹

1092

1093

¹Institut de Physique du Globe de Paris, Sorbonne Paris Cité, Université Paris Diderot, UMR 7154 CNRS, F-75005 Paris, France

1094

1095

²Total EP CSTJF, Pau, France

1096

³Laboratoire Biogéosciences, UMR 6282, CNRS, Université Bourgogne Franche-Comté, 21000 Dijon, France

1097

⁴IFP Energies Nouvelles, 1-4 Avenue de Bois Préau, 92852, Rueil-Malmaison Cedex, France

1098

⁵Total EP Bolivia

1099

Corresponding author: Elodie Muller (emuller@ipgp.fr)

1100

1101

Analytical methods

1102

N₂ gas: $\delta^{15}\text{N}$ of N₂ gas was measured following the protocol of Li et al. (2009). Purification starts with a cryogenic separation at liquid nitrogen temperature. The non-condensable gases, including N₂, H₂, O₂, CH₄ and He, are inserted in the line and circulated using a mercury Toeppler pump through a CuO reactor maintained at 950 °C for 30 minutes (and then cooled to 450 °C) to oxidize H₂ and CH₄. The resulting CO₂ and H₂O are cryogenically trapped at liquid-nitrogen boiling temperature. Excess O₂, if any, is resorbed and the NO_x that was potentially generated during the previous oxidation phase is reduced to N₂ by circulating the gases over a Cu reactor maintained at 600 °C. The purified N₂ and He are then collected with the mercury Toeppler pump and manometrically quantified before being transferred in vials for measurement using a dual-inlet IRMS Delta + XP. This instrument is calibrated by measuring an internal reference N₂ gas, itself calibrated against the air, the international reference standard for $\delta^{15}\text{N}$ measurements, which has by definition an absolute value of $\delta^{15}\text{N}_{\text{Air}} = 0\text{‰}$. The CO₂ that was trapped using liquid nitrogen was then released at -140 °C, collected using a liquid N₂ trap and manometrically quantified before being transferred to vials for measurement using the dual-inlet IRMS Delta + XP. $\delta^{13}\text{C}$ values compare well with those obtained by GC/C/IRMS at the IFPEN laboratory (mean difference < 0.2‰; Table A1).

1109

Noble gas: Noble gases were measured following the protocol of Moreira et al. (2018). The gas purification consists of several combustions: the first one with a Bulk Getter (SAES) heating system maintained at 400 °C for 5 minutes, followed by two 5-minute combustions at 800 °C each with titanium sponge. After purification, helium is separated from the other noble gases using activated charcoal at 30 K, introduced into the Helix-SFT mass spectrometer and analyzed using peak jumping. ³He is collected on the electron multiplier in pulse-counting mode whereas ⁴He is analyzed on the Faraday cup and the signal is amplified using either 10¹¹ ohm or 10¹² ohm resistance depending on the signal. After the helium was measured, neon is released from the cold trap at 70 K. Two

1127

cycles of neon isotope measurement are performed before neon is introduced to stabilize the magnet. For each cycle, ^{20}Ne is measured using a mass-scan instead of setting the magnet on the required field to measure ^{20}Ne (see Moreira et al., 2018 for details). ^{21}Ne , ^{22}Ne , ^{40}Ar and CO_2 were measured for 10 seconds each using peak switching. Argon is partially desorbed at 130 K and transferred to charcoal at the temperature of liquid nitrogen for 15 minutes. After the desorption of argon at room temperature from the charcoal trap, dilution(s) using a 1 L reservoir is/are used to decrease the amount of argon introduced into the mass spectrometer. ^{36}Ar and ^{38}Ar are collected on the electron multiplier, whereas ^{40}Ar is measured on the Faraday cup using 10^{11} ohm resistance. All the data were corrected following the procedure of Moreira et al. (2018).

B isotopes: $\delta^{11}\text{B}$ was measured in rock samples following the protocol of Chetelat et al. (2009). Finely powdered sample (50 mg) was admixed with 300 mg of ultra-pure K_2CO_3 in a Pt crucible and melted in a muffle furnace at 950 °C for 15 minutes. The pellet was taken up in 3 mL of 0.5 HNO_3 and added to a 50 mL vial filled with 20 mL H_2O . An additional 1-2 mL of 0.5N HNO_3 were added until complete dissolution. The final pH was adjusted to pH 1.7 with 3N HNO_3 , and 7 mL of this solution were passed through 2 mL of the cation exchange resin AG 50W-X8 to extract most of the cationic load. The recovered solution was adjusted to pH 8-9 with distilled 4N NH_4OH and B was extracted on Amberlite IRA-743 resin in two steps: the first step consisted of extraction on a column loaded with 300 μL of resin and the second step of purification (after adjustment to pH 8-9 again) on a column filled with 50 μL of the resin.

Geothermometric calculations

The silica concentration of our samples is fairly uniform within the range of 101 to 154 mg/l (Table 2). Applying the quartz geothermometer described in Kharaka and Mariner (1989), Verma and Santoyo (1995, 1997) estimated equilibrium temperatures of spring water with the rocks of a deep reservoir up to 163 ± 3 °C (assuming no steam loss; Table A3) with a mean of 149 ± 11 °C. However, considering the temperature between the surface and the deep reservoir, the strong influence of temperature on quartz solubility as well as precipitation of silica during water cooling as it ascends to the surface could affect the estimated temperature. The Na-K-Ca geothermometer yields similar estimates (156 ± 30 °C) when the Mg correction of Fournier and Potter (1979) is applied. But similarly, this geothermometer calibrated on silicates can also be affected by a precipitation of silicates during the cooling of the thermal water.

The Na-Li geothermometer gives much higher estimates (around 300 °C) regardless of the equation used (Fouillac and Michard, 1981; Kharaka et al., 1982; Verma and Santoyo, 1993, 1997). Using a larger dataset than in the previous articles, Sanjuan et al. (2014) modified the equations of Kharaka et al. (1982) and Fouillac and Michard (1981). Their corrections do not modify the results for the Kharaka et al. equation (mean value 325 °C) and decrease the values obtained with the Fouillac and Michard equation (mean value 251 °C) by 50 °C. The Li-Mg geothermometer (Kharaka and Mariner, 1989) yields lower values (186 ± 18 °C; Table A3) than the Na-Li geothermometer. The discrepancies observed between the geothermometers using Li can be explained by the high concentrations of Li in our samples. The $\text{Log}(\text{Na}/\text{Li})$ values obtained for the thermal springs of Laguna Pastos Grandes are between 1.24 and 1.47 whereas the values used by Sanjuan et al. (2014) for their calibrations are never lower than 2.00. Consequently, our

data are not in the range of calibration of the equations and if the correlations cannot be extended linearly, the uncertainties on the calculated temperatures will be high.

The geothermometer based on Li isotopes was also tested as it is independent from the Li concentration. This geothermometer was calibrated experimentally on springs from the Guadeloupe and Martinique volcanic arcs (Millot et al., 2010). It relies on the fact that Li isotopic fractionation ($\Delta_{\text{solution-solid}}$) between solution and basalt is strongly temperature dependent with, for example, values of +19.4‰ at 25 °C to 6.7‰ at 250 °C. Considering the $\delta^7\text{Li}$ mean value of 4.44 ± 0.90 ‰ for thermal springs and using the values for rhyolitic ignimbrite, dacite and andesite in the area that are reported in Table 3, we obtained a $\Delta_{\text{solution-solid}}$ of 8, 10 and 12‰, respectively. Knowing that the Central Andes Ignimbrites are a 50:50 mixture of mantle-derived basalts and of regional crust (de Silva and Kay, 2018), we can hypothesize that the behavior of Li in these rocks and in the altered products is not very different from that in the andesite of Guadeloupe. In this case, the calibration temperature of Millot et al. (2010) for fractionations between 8 and 12‰ would give a temperature of 200 ± 25 °C. The Na-K geothermometer yields similar estimates of 228 ± 9 °C with the equation of Verma and Santoyo (1997) and 205 ± 12 °C with that of Santoyo and Diaz-Gonzalez (2010).

PHREEQC modeling:

The mineralogical composition of the volcanic rocks sampled around the Laguna Pastos has been determined by DRX as:

- Dacite: alkali and potassium feldspar, quartz, biotite
- Andesite: alkali feldspar, biotite, olivine, amphibole
- Ignimbrite: alkali and potassium feldspar, quartz, biotite, amphibole

As numerous of these minerals are not available in the Thermoddem database, we performed the PHREEQC modeling with the selected minerals as follows:

Solution 1

units mmol/l

temp 225 # Temperature varying between 200 and 250 °C

Equilibrium_phases 1

Quartz(alpha) 0.0 10.0

Sanidine 0.0 10.0

Albite(low) 0.0 10.0

Anorthite 0.0 10.0

Pargasite 0.0 10.0

Anhydrite 0.0 10.0

CO2(g) 1.3 #CO2(g) SI varying between 1-2

Halite 0.0 0.239 #Corresponding to the average Cl concentration in

End spring water

References

- Fouillac C. and Michard G. (1981) Sodium/lithium ratio in water applied to geothermometry of geothermal reservoirs. *Geothermics* **10**(1), 55-70.
- Fournier R. O. and Potter Ii R. W. (1979) Magnesium correction to the Na/K/Ca chemical geothermometer. *Geochimica et Cosmochimica Acta* **43**(9), 1543-1550.
- Kharaka Y. K., Lico M. S. and Law L. M. (1982) Chemical geothermometers applied to formation waters, Gulf of Mexico and California basins. *AAPG Bulletin* **66**(5), 588-588.

Kharaka Y. K. and Mariner R. H. (1989) Chemical geothermometers and their application to formation waters from sedimentary basins. In *Thermal history of sedimentary basins*. Springer, New York, NY. pp. 99-117.
Verma S. P. and Santoyo E. (1995) New improved equations for Na/K and SiO₂ geothermometers by error propagation. *Proc. World Geotherm. Congr* **2**, 963-968.

Figure captions

Figure A1. Photography and illustrating schema of bubbling gas sampling method.

Figure A2. Comparison of the water composition obtained for the volcanic bedrock weathering at 200 (blue), 225 (red) and 250 °C (green) with increasing pCO₂ from 10 bar in light color to 100 bar in dark color. The average spring water is in black.

Figure A3. Air-normalized helium R/Ra values plotted against He/Ne ratios of gas samples from Laguna Pastos Grandes compared with other Andean sources (Hoke et al., 1994). Mixing lines between the three main sources of helium (crustal CRUST, mantle MORB and air saturated water ASW) are also represented.

Figure A4. Relations between chloride and sodium for Pastos Grandes brines (in yellow) and water sources as a function of temperature: thermal spring >35 °C in red, <32 °C in orange and cold stream <15 °C in blue. Na-Cl compositions are compared with other Bolivian salars (pale triangles; Risacher and Fritz, 1991). Data from this study are reported with dots and previous data with squares (Ballivian and Risacher, 1981; Hurlbert and Chang, 1984; Risacher and Fritz, 1991; Jones and Renaut, 1994).

1246 **Table A1.** Detailed nitrogen and carbon isotopic analysis of gas samples from Laguna
1247 Pastos Grandes.

Nitrogen analysis				
Sample	Date	Method	$\delta^{15}\text{N}$ (‰)	1 σ
PG100	20/07/2017	GC-IRMS on steel tube	2.73	0.03
PG100	20/07/2017	GC-IRMS on steel tube	2.75	0.01
PG112	20/07/2017	GC-IRMS on steel tube	1.79	0.02
PG112	20/07/2017	GC-IRMS on steel tube	1.77	0.01
PG112	07/02/2018	GC-IRMS on exetainer	1.74	0.02
PG116	07/02/2018	GC-IRMS on exetainer	1.60	0.02
PG117	19/07/2017	GC-IRMS on steel tube	2.49	0.05
PG117	19/07/2017	GC-IRMS on steel tube	2.47	0.03
PG117	19/07/2017	GC-IRMS on steel tube	2.24	0.03
PG117	19/07/2017	GC-IRMS on steel tube	2.26	0.02
PG117	19/07/2017	GC-IRMS on steel tube	2.18	0.02
PG117	19/07/2017	GC-IRMS on steel tube	2.17	0.02
Carbon analysis				
Sample	Date	Method	$\delta^{13}\text{C}$ (‰)	1 σ
PG100	14/06/2017	GC-C-IRMS	-11.36	0.01
PG100	14/06/2017	GC-C-IRMS	-11.32	0.01
PG100	14/06/2017	GC-C-IRMS	-11.31	0.01
PG100	20/07/2017	GC-IRMS	-10.73	0.03
PG100	20/07/2017	GC-IRMS	-11.27	0.03
PG112	14/06/2017	GC-C-IRMS	-11.31	0.01
PG112	14/06/2017	GC-C-IRMS	-11.24	0.01
PG112	14/06/2017	GC-C-IRMS	-11.26	0.01
PG112	20/07/2017	GC-IRMS	-11.11	0.03
PG112	20/07/2017	GC-IRMS	-11.24	0.03
PG116	14/06/2017	GC-C-IRMS	-11.25	0.03
PG116	14/06/2017	GC-C-IRMS	-11.08	0.03
PG116	14/06/2017	GC-C-IRMS	-11.05	0.03
PG116	07/02/2018	GC-IRMS	-11.00	0.04
PG116	07/02/2018	GC-IRMS	-11.49	0.04
PG116	07/02/2018	GC-IRMS	-11.43	0.06
PG117	14/06/2017	GC-C-IRMS	-11.06	0.04
PG117	19/07/2017	GC-IRMS	-10.85	0.05

Table A2. Stable isotope compositions of Andean salars water, rainfall and snow from the region of Pastos Grandes (from this study* and Boschetti et al., 2007).

	$\delta^{18}\text{O}$ ($\pm 0.1\text{‰}$, 1s)	δD ($\pm 0.8\text{‰}$, 1s)
Chaxa lagoon	-0.8	-30.5
Miñique lagoon	5.4	10.1
Miscanti lagoon	3.3	0.5
Uyuni*	1.9	-26.1
Rainfall*	-16.3	-112.9
Snow 1*	-6.8	-30.3
Snow 2*	-2.7	6.5

Table A3. Estimated equilibrium temperatures ($^{\circ}\text{C}$) for hydrothermal sources obtained with different geothermometers.

Geothermometer	PG_117	PG_112	PG_100	PG1_1	MV_1	PGS_1	Mean	1s
SiO_2 (Verma and Santoyo, 1997)	145	138	145	163	162	138	149	11
Na/K/Ca – Mg (Fournier and Potter, 1979)	177	144	169	167	171	107	156	26
Na/K (Verma and Santoyo, 1997)	215	226	237	222	230	240	228	9
Na/K (Santoyo and Diaz-Gonzalez, 2010)	188	202	216	197	221	207	205	12
Na/Li (Fouillac and Michard, 1981)	315	316	344	272	283	268	300	30
Na/Li (modified by Sanjuan et al., 2014)	264	264	285	230	239	226	251	23
Na/Li (Verma and Santoyo, 1997)	323	324	351	280	292	276	308	30
Na/Li (Kharaka et al., 1982)	334	335	353	304	312	301	323	21
Na/Li (modified by Sanjuan et al., 2014)	336	337	355	306	314	303	325	21
Mg/Li (Kharaka and Mariner, 1989)	199	193	197	185	192	151	186	18

Table A4. $\delta^{37}\text{Cl}$ analyses of water samples from Laguna Pastos Grandes.

Sample	$\delta^{37}\text{Cl}$ (‰)	1 σ
La Salsa 1	0.308	0.002
La Salsa 2	0.230	0.010
La Salsa 3	0.230	0.009
La Salsa 4	0.260	0.009
La Salsa 5	0.234	0.003
La Salsa 6	0.292	0.002
La Salsa 7	0.300	0.002
La Rumba 1	0.227	0.010
La Rumba 2	0.205	0.006
La Rumba 3	0.234	0.011
El Ojo Verde 1	0.246	0.009
El Ojo Verde 2	0.252	0.013
Average	0.251	0.032

1255 **Table A5.** Results of PHREEQC modeling. Alb. Albite(low); Anh. Anhydrite; An. Anorthite;
1256 Hal. Halite; Par. Pargasite; Qtz. Quartz(alpha); San. Sanidine

pCO ₂ (bar)		Alb.	Anh.	An.	CO2(g)	Hal.	Par.	Qtz	San.	C Ca Cl K					
Input temperature: 200 °C	10	Amount of dissolution (-) or precipitation (+) (molality)	4.9E-2	-5.0E-4	-1.7E-2	-1.0E-1	-2.4E-1	-1.4E-3	-7.6E-2	-1.1E-2	Water chemistry (molality)	1.0E-1	2.0E-2	2.4E-1	1.1E-2
	20		5.0E-2	-5.3E-4	-1.6E-2	-2.0E-1	-2.4E-1	-2.4E-3	-7.6E-2	-1.1E-2		2.0E-1	2.1E-2	2.4E-1	1.1E-2
	40		5.2E-2	-5.7E-4	-1.4E-2	-3.9E-1	-2.4E-1	-4.4E-3	-7.4E-2	-1.1E-2		3.9E-1	2.3E-2	2.4E-1	1.1E-2
	60		5.4E-2	-6.0E-4	-1.2E-2	-5.8E-1	-2.4E-1	-6.3E-3	-7.2E-2	-1.1E-2		5.8E-1	2.5E-2	2.4E-1	1.1E-2
	80		5.5E-2	-6.3E-4	-9.9E-3	-7.6E-1	-2.4E-1	-8.1E-3	-6.9E-2	-1.1E-2		7.6E-1	2.7E-2	2.4E-1	1.1E-2
	100		5.7E-2	-6.6E-4	-7.8E-3	-9.6E-1	-2.4E-1	-1.0E-2	-6.7E-2	-1.1E-2		9.6E-1	2.9E-2	2.4E-1	1.1E-2
Input temperature: 225 °C	10		3.6E-2	-4.5E-4	-9.4E-3	-1.0E-1	-2.4E-1	-6.4E-4	-4.7E-2	-1.5E-2		1.0E-1	1.1E-2	2.4E-1	1.5E-2
	20		3.6E-2	-4.7E-4	-8.9E-3	-2.0E-1	-2.4E-1	-1.1E-3	-4.6E-2	-1.5E-2		2.0E-1	1.2E-2	2.4E-1	1.5E-2
	40		3.7E-2	-4.9E-4	-8.1E-3	-4.0E-1	-2.4E-1	-1.9E-3	-4.5E-2	-1.5E-2		4.0E-1	1.2E-2	2.4E-1	1.5E-2
	60		3.7E-2	-5.1E-4	-7.2E-3	-6.0E-1	-2.4E-1	-2.7E-3	-4.4E-2	-1.5E-2		6.0E-1	1.3E-2	2.4E-1	1.5E-2
	80		3.8E-2	-5.2E-4	-6.3E-3	-7.9E-1	-2.4E-1	-3.4E-3	-4.3E-2	-1.5E-2		7.9E-1	1.4E-2	2.4E-1	1.5E-2
	100		3.8E-2	-5.4E-4	-5.4E-3	-9.9E-1	-2.4E-1	-4.2E-3	-4.1E-2	-1.5E-2		1.0E0	1.4E-2	2.4E-1	1.5E-2
Input temperature: 250 °C	10		3.2E-2	-4.3E-4	-5.8E-3	-1.1E-1	-2.4E-1	-3.0E-4	-3.1E-2	-1.9E-2		1.1E-1	6.8E-3	2.4E-1	1.9E-2
	20		3.2E-2	-4.4E-4	-5.6E-3	-2.2E-1	-2.4E-1	-5.0E-4	-3.1E-2	-1.9E-2		2.2E-1	7.0E-3	2.4E-1	1.9E-2
	40		3.2E-2	-4.5E-4	-5.2E-3	-4.5E-1	-2.4E-1	-8.6E-4	-3.0E-2	-1.9E-2		4.5E-1	7.3E-3	2.4E-1	1.9E-2
	60		3.3E-2	-4.6E-4	-4.8E-3	-6.7E-1	-2.4E-1	-1.2E-3	-3.0E-2	-1.9E-2		6.7E-1	7.6E-3	2.4E-1	1.9E-2
	80		3.3E-2	-4.7E-4	-4.4E-3	-8.8E-1	-2.4E-1	-1.5E-3	-2.9E-2	-1.9E-2		8.9E-1	7.9E-3	2.4E-1	1.9E-2
	100		3.3E-2	-4.7E-4	-4.0E-3	-1.1E0	-2.4E-1	-1.8E-3	-2.9E-2	-1.9E-2		1.1E0	8.2E-3	2.4E-1	1.9E-2

1257
1258

Table A6. Comparison of Laguna Pastos Grandes characteristics with Chilean and Bolivian salars. Data from this study and Hoke et al., 1994; Spiro et al., 1997; Risacher et al., 2003, 2011; Risacher and Fritz, 1991, 2009. ul: ulexite; hal: halite; gyps: gypsum; mirab: mirabilite. *Previous data TDS: Total Dissolved Solids

	Laguna Pastos Grandes	Chilean salars	Bolivian salars
Location	Bolivian Altiplano	Western Cordillera	Bolivian Altiplano
Basement	Dacite-Andesite- Rhyolitic Ignimbrite	Rhyolitic ignimbrite Andesite	Andesite Rhyodacite
Altitude	4450 m	3400-4300 m	4100-4600 m
Surface	130 km ²	0.03-400 km ²	0.03-500 km ²
Potential evaporation	1400 mm/year	1000-2000 mm/year	1000-1500 mm/year
Precipitation	100 mm/year	40-380 mm/year	50-150 mm/year
Mean temperature	5 °C	0 °C	5-10 °C
Morphology	Playa lake	Mainly playa lakes	Mainly playa lakes
Salinity	256 g/l	1.2-365 g/l	0.4-348 g/l
Brine type (<i>Na-Cl-</i>)	Ca	65% SO ₄ – 24% Ca	52% SO ₄ – 26% CO ₃ – 19% Ca
Salts	Calcite-gyps.-ul.-hal.	Gyps.-hal.-mirab.-ul.	Gyps.-hal.-mirab.-ul.
Infiltration rate	~negligible	0.01-12.8% of outflow	0.01% - ~inflows
Thermal influence (<i>T</i> >15°C)	Yes	78 %	60%
Spring T _{max}	47 °C (20-75 °C*)	83 °C (Puchuldiza)	36 °C (Challviri)
Spring TDS (range)	14 g/l	3.8 g/l in average (0.2-21.8)	0.82 g/l in average (max. 14)
Mantle influence	47%	69%	44%
CO ₂ isotopic composition	-11‰	-8 to -0.6‰	-20 to -6‰